The free oscillatory response of fjord-type multi-armed lakes

by

Samuel Brenner

B.A.Sc., The University of British Columbia, 2015

A THESIS SUBMITTED IN PARTIAL FULFILLMENT OF
THE REQUIREMENTS FOR THE DEGREE OF

MASTER OF APPLIED SCIENCE

in

The Faculty of Graduate and Postdoctoral Studies

(Civil Engineering)

THE UNIVERSITY OF BRITISH COLUMBIA

(Vancouver)

August 2017

Abstract

This study examines the structure and frequency of free seiche modes in fjord-type multi-armed lakes in order to generalize features of the response of those lakes. The effect of multiple arms on seiches within a lake is not easy to predict. To do so, this study develops a simplified analytical model (SAM) based on idealized lake geometries. In addition, a characterization of surface (barotropic) modes is compared for two "Y-shaped" lakes: Quesnel Lake in Canada, and Lake Como in Italy. Lake Como and Quesnel Lake are studied through a combination of field observations and modelling, both numerically using a Finite Element Method (FEM) scheme and using SAM.

SAM demonstrates that multi-armed lakes are subject to two classifications of behaviour: a full-lake response, in which all arms are active; and a decoupled response, in which seiching is constrained to only two arms of the lake. A geometric parameter in each arm, which represents the travel time of a progressive shallow-water wave in that arm, determines the range of behaviours expressed: each lake will either experience only a whole-lake response or it will exhibit alternating whole-lake and decoupled modes.

The behaviour predicted by SAM is consistent with modes observed and predicted in both Quesnel Lake and Lake Como. Modal periods are identified from observed water level measurements using spectral analysis. FEM predicted periods agree with observations. SAM correctly reproduces the periods of the lowest frequency modes in both lakes when a constant depth is used for each arm. Mode-shapes predicted by SAM qualitatively match those given by the FEM model. While all modes of Quesnel Lake are whole-lake modes, some of the modes in Lake Como exhibit a decoupled response. The results given here also support generalization of the fundamental mode as being inherently the same structure as Merian-type modes in simple elongated lakes.

While the study focusses on barotropic modes, SAM can be similarly applied to internal (baroclinic) modes, and so the general behaviours observed here are appropriate for describing both the barotropic and baroclinic responses of multi-armed lakes.

Lay Summary

Wind forcing along the surface of a lake pushes water to the downwind end. When the wind forcing is released, this water mass rocks back and forth in a motion called seiching. Accompanying this oscillation of the water surface are oscillations of the currents within the lake, which are important for the overall transport of material. While these oscillations can be described very well in simple lakes, when lakes have multiple arms we can no longer make general statements about this seiching. This study uses a combination of theoretical work and case studies to better describe seiching in multi-armed lakes. The results of the study identify that for certain geometries the seiche response will be constrained to only a subset of arms of the lake.

Preface

The work presented here represents original research carried out by the author under the supervision of B. Laval (University of British Columbia). The thesis is presented as two manuscripts (Chapters 2 and 3), with Chapter 1 providing relevant background and motivation for both. Chapter 4 provides overall conclusions and identifies opportunities for further work. A second reader, G. Lawrence (University of British Columbia), provided valuable comments on drafts of this work. The contributions of co-authors are as follows:

A version of Chapter 2 is being prepared for submission to a peer-reviewed journal as "Development of an analytical solution for seiche modes in fjord-type multi-armed lakes" by S. Brenner, and B. Laval. I was the lead investigator for this work, and completed all manuscript preparation. B. Laval is acting in a supervisory role and is providing critical feedback and ongoing editing of the manuscript.

Portions of Chapter 3 will also be submitted for publication; however, additional work will need to be completed before this is possible. As such, the final title and author list is still under discussion. In its current form, all analysis and manuscript preparation in Chapter 3 was completed by myself. The field study of Quesnel Lake presented in Chapter 3 was developed and deployed by B. Laval and S. Vagle (Institute of Ocean Sciences) as part of a wider study before the onset of this thesis work; however, I assisted with retrieval of field data and performed all relevant analysis for this work. B. Laval is acting in a supervisory role in this endeavour and was involved throughout the project in concept formation and manuscript edits. An additional researcher, J. Shore (Royal Military College of Canada), performed modelling work of Quesnel Lake. That work is not presented in the current document, but comparisons have been made with the relevant observations and modelling presented in Chapter 3 and so her work has helped to verify the results here.

Table of Contents

List of Tables

List of Figures

Acknowledgements

I could not have completed this work without the help and support of my friends and family. I am especially grateful to Angie, whose exceptional patience and understanding through the past two years has been instrumental in my success.

For helping with the study of Quesnel Lake, I'd like to thank Svein Vagle, Brody Granger, and Andrew Hamilton who spent a week with me on the lake performing fieldwork, and the researchers at the Quesnel River Research Institute for hosting us. I'd also like to thank Jennifer Shore who provided feedback and ideas about Quesnel Lake, who ran through many model runs based on hunches I had, and who postponed her own publication submission so that we could work together. Stephen Déry provided atmospheric data when I was still hoping to link seasonal wind regimes to variations in Quesnel Lake's response, and his student, Hadleigh Thompson, is happily taking on the task of trying to better describe the spatial wind patterns in the region so that someone else might solve that problem.

The inclusion of Lake Como in this thesis is due to the generosity of Giulia Valerio and Marco Pilotti in sharing their data.

I appreciate the discussions, the exchanges of ideas and problems, and the camaraderie with the other students in both the Environmental Fluid Mechanics and the Physical Oceanography groups at UBC. In particular, David Hurley, Mark Sumka, Kelly Graves, and Brody Granger deserve recognition.

I've benefited immensely from the support of professors and researchers in both Civil Engineering and Oceanography. In particular Greg Lawrence, Rich Pawlowicz, Ted Tedford, and Andrew Hamilton have helped me work through numerous questions. Of course, the professor to whom I owe the most thanks is my supervisor, Bernard Laval, who read through many iterations of this work and provided a great deal of critical feedback and encouragement, and who supported me most by sharing my curiosity.

This work has been partially supported by an NSERC CGS-M award and Environment and Climate Change Canada's Environmental Damages Fund.

Chapter 1

Introduction

1.1 Motivation

Basin-scale standing wave oscillations in enclosed or semi-enclosed basins are a ubiquitous feature in both natural and man-made water bodies. Standing-wave oscillations (or "seiches") occur on both the water surface and the internal temperature distribution, and both are accompanied by out-of-phase oscillations of the horizontal velocity field. Many early studies in the field of physical limnology were attempts to better understand and explain the phenomenon of seiching. From the end of the 19^{th} and beginning of the 20^{th} century, a number of publications on the subjects of both surface and internal seiching (at that time called "temperature seiching") in the Scottish Lochs were produced by the Scottish Lake Survey (e.g. Murray, 1888; Watson, 1904; Wedderburn, 1907). These came at a time when oceanographers were working to better understand tidal waves in semi-enclosed seas (e.g. Defant, 1918; Proudman, 1915). The connection between these problems allowed for a great deal of understanding of these processes, and formed a basis for the current theory of seiches. With modern computer technology and the advancement of fully three-dimensional hydrodynamic models, researchers now have the ability to accurately resolve many aspects of lake motion, including the seiche response. As a result, questions about seiches have largely shifted from understanding the shapes and periods of these seiches to understanding their impacts on the processes such as mixing and transport of materials within lakes.

Nonetheless, there are still aspects of seiching that are not fully understood. Despite being able to fully resolve wave modes and periods using two- and three-dimensional models, there is not always a satisfying explanation of *why* some features exist in the response of complex lakes. The early studies by the Scottish Lake Survey developed mathematical explanations for seiche motions in glacially-carved "fjord-type" lakes. These lakes are typically steep-sided and deep, and, importantly, they are long and narrow. This simple geometry allows for the equations of motion to be applied along the longitudinal axis of the lake so transverse motions can be ignored. The

resulting reduction of dimension allows for the governing partial differential equations (PDEs) to be converted to a more tractable set of ordinary differential equations (ODEs), which are simpler to both solve and explain. For basins whose surface geometry cannot be readily approximated as one-dimensional, the seiche response is necessarily predicted by a set of PDEs that do not provide results that are intuitive, nor are they easy to generalize. The study of lakes that have features such as bays, sub-basins, or multiple arms are thus described in a case-by-case approach that doesn't necessarily provide any predictive power or understanding of other lakes with similar features.

Here, a particular class of complex lakes is investigated: multi-armed fjord-type lakes. By considering fjord-type lakes specifically, this study will restrict the range of possible motions to focus on the impact on the lake response of multiple arms alone without having to consider transverse or rotational motions. In so doing, some generalized behaviours of this geometric feature can be described. Before proceeding with the study, the following section provides a review of literature describing the background and mathematical formulation of the processes discussed through the remainder of the thesis.

1.2 Review of relevant literature

1.2.1 Standing waves in basins of simple geometry

Seiching in lakes was perhaps first seriously described by Forel's 19th century works on Lake Geneva (Defant, 1960; Hutter et al., 2010; Wilson, 1972). However, this phenomenon was previously measured as far back as the 16th century (Wilson, 1972) and throughout both Europe and North America from the 17th century onwards (Chrystal, 1905). Since these early accounts, seiching (particularly baroclinic seiching) has been considered to be one of the primary mechanisms for mass transport in lakes and has been the subject of numerous studies. In addition to the many journal publications on the topic, this physical process is also featured in sections of textbooks on the subjects of both limnology (e.g. Wetzel, 1983) and oceanography (e.g Defant, 1960; LeBlond and Mysak, 1978; Proudman, 1953), and in one case is the subject of an entire textbook volume (Hutter et al., 2011). Given the history and volume of work on this subject, it is infeasible to provide a full account of all of these works. Presented in the sections below is a description of the physical process and a summary of seminal works on both barotropic and baroclinic seiching.

Seiching refers to the standing-wave response of an enclosed or semi-

enclosed basin to some pressure imbalance. After the driving mechanism that creates this imbalance is removed the lake attempts to return to some equilibrium position, but instead this position is overshot and a new pressure imbalance appears. This process repeats and the lake oscillates. In the case of surface (barotropic) seiching, this takes the form of an oscillation of the free surface accompanied by an out-of-phase oscillation of the mean horizontal velocity (Figure 1.1a). Most lakes exhibit seasonal thermal stratification with a sharp temperature gradient (the thermocline) separating the surface (epilimnion) and deep water (hypolimnion). This temperature interface responds to a surface pressure imbalance by deflecting the opposite direction; when the pressure imbalance is allowed to relax, standing wave oscillations of the interface occur. The out-of-phase two-layer circulation generated by these internal (baroclinic) seiches creates a shear flow with mean epilimnetic and mean hypolimnetic velocities having opposite sign (Figure 1.1b). In describing these processes, we first consider these oscillatory motions in lakes of "simple" geometry, which refer to lakes that are sufficiently long and narrow such that transverse motions and effects from the Earth's rotation are negligible compared to longitudinal motions, and these lakes are devoid of complicating factors such as bays, sub-basins, or multiple arms.

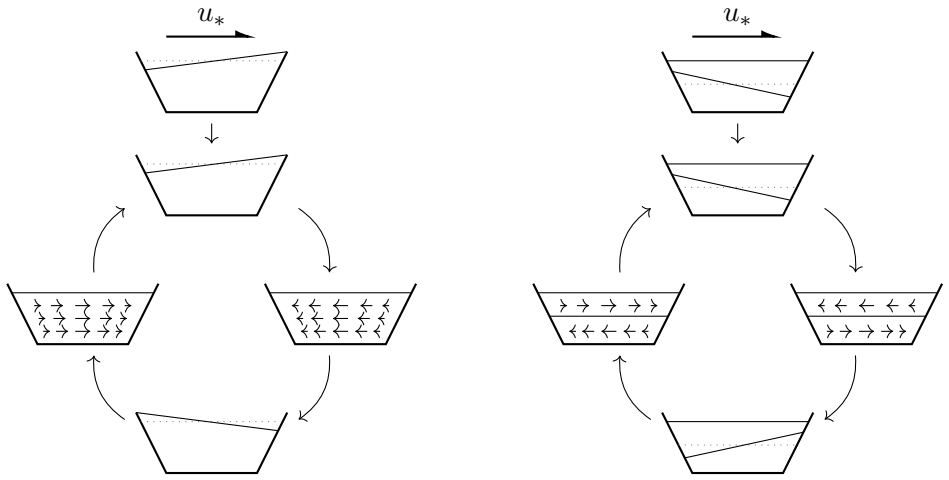

(a) Barotropic seiching **(b)** Barolinic seiching

Figure 1.1: Schematic of the evolution of (a) a surface (barotropic) seiche in a homogeneous water body, and (b) an internal (baroclinic) seiche in two-layer system. After the forcing is removed, the surface/interface deflection and the water column velocity both oscillate, but are out of phase both spatially and in time

Barotropic seiches

While barotropic seiching is a response to some pressure imbalance or excitation, the driving force that creates the imbalance is not strictly defined. Defant (1960) lists a number of possible forcing mechanisms for seiches:

1. The sudden return to its equilibrium of a surface previously disturbed by the passage of an atmospheric disturbance over a section of the lake
2. The sudden oscillation back to a state of equilibrium of a watermass previously piled up by wind
3. Sudden or rapid receding of an accumulation of water produced by an extremely rapid influx across a section of the lake (violent rainfalls).
4. Shocks of rain drops falling on the water surface.
5. Sudden changes in air pressure.
6. Shock pressures of wind gusts on the lake surface.
7. Subsiding of the electrical attraction on the surface by thunder clouds.

These are roughly the same set of mechanisms previously identified by Wedderburn (1922, conveying the findings of various works by Chrystal), though his list does not include mechanism (7) and it separates mechanism (6) into: "the effect of squalls", "impact of wind gusts", and periodic fluctuations in the wind. Aside from it's inclusion in the list, Defant (1960) provides no information for mechanism (7), and this does not appear in other prominent works. In addition to the list provided by Defant (1960), other set-up mechanisms exist:

8. Seismic activity (suggested by Chrystal (1905, 1908), and shown definitively in more recent works (e.g Barberopoulou, 2008; Pieters and Lawrence, 2014))
9. Landslides (e.g. Balmforth et al., 2009; Kulikov et al., 1996)
10. Tidal forcing (especially in large lakes; e.g. Hamblin, 1974)

Chrystal (1908) agrees with an earlier statement by Forel (as cited in Defant, 1960) that changes in atmospheric pressure (mechanisms 1 and 5) are the most frequent causes of seiching, with the influence of wind (mechanisms 2 and 6) being less important. Wedderburn (1922) states that there is no evidence of piling up of water at the downwind of the lake as would be required for (2), except for very shallow lakes. Despite this claim, modern theory often supports mechanism (2) as the cause of surface seiching. This shift in view may be due to the relationship of this mechanism to understanding of the

set-up of baroclinic seiching (Mortimer, 1952; Stevens and Imberger, 1996). The driving force determines which of the possible seiche modes are excited, but otherwise does not define the characteristic shapes or periods of those modes. The mode characteristics are a property of the lake geometry itself.

Merian (1828, as cited in Chrystal, 1905) developed a formula for the periods of longitudinal free oscillations in a rectangular basin of length L and constant depth H:

$$T_n = \frac{2L}{n\sqrt{gH}} \tag{1.1}$$

where it is recognized that the term $\sqrt{gH}$ in the denominator is the wave speed of a shallow water wave. However, this formula was not connected to seiching until Forel (1876, as cited in Chrystal, 1905) suggested that it could be applied to predict the resonant periods of lakes. Merian's formula is now ubiquitous in modern works.

In the early part of the 20$^{\text{th}}$ century, many advances in the understanding of seiching were made by Chrystal working with the Scottish Lake Survey (e.g Chrystal, 1905, 1908; Chrystal and Murray, 1907; Chrystal and Wedderburn, 1905). In particular, Chrystal sought to describe the influence of cross-sectional variation on the sequence of modal periods and the location of nodes. To this end, Chrystal (1905) presented an equation to describe the free evolution of the depth-integrated horizontal velocity ($q = \int_0^H u dz$) of a lake in terms of variations in cross-sectional area, $S(x)$, and width at the surface, $b(x)$:

$$\frac{\partial^2 \Xi}{\partial t^2} = g\sigma(\chi)\frac{\partial^2 \Xi}{\partial \chi^2},$$

where

$$\Xi = S(x)q(x,t), \quad \chi = \int_0^x b(s)ds, \quad \text{and} \quad \sigma = S(x)b(x).$$

He called the graph with χ on the x-axis and σ on the y-axis the "normal curve" of a lake. In the case of constant width $b(x) = b$, and varying depth $H(x)$, this reduces to the more familiar

$$\frac{\partial^2 q}{\partial t^2} = gH(x)\frac{\partial^2 q}{\partial x^2}. \tag{1.2}$$

A corresponding equation can be developed for the deflection of the free surface $h(x,t)$:

$$\frac{\partial^2 h}{\partial t^2} = g\frac{\partial}{\partial x}\left[H(x)\frac{\partial h}{\partial x}\right] \tag{1.3}$$

These equations rely on the assumption that $h \ll H$, and are thus "linearised". For barotropic motions, this assumption is typically valid; however, it may not be so for baroclinic motions.

Chrystal (1905) then developed a series of mathematical functions which he named "Seiche-sine", "Seiche-cosine", and the "Lake Function" which solve Equation 1.2 for certain analytically defined bottom profiles. Halm (1905) shows that these functions are a part of a broader class of hypergeometric functions, and are not only of value in understanding lakes but can be used to help solve other equations in the field of applied mathematics.

Despite Chrystal's success in solving Equation 1.2 for analytically defined profiles, it was found that many lake geometries can not be easily defined by such profiles. As a result, researchers such as Proudman (1915) and Defant (1918, as cited in Defant, 1960; Mortimer, 1979) developed numerical methods to solve Equations (1.2) and (1.3) for arbitrary profiles. Defant (1960) presents these together with the analytical method developed by Chrystal (1905) and a number of similar methods proposed by other researchers. Between these methods, reasonably accurate approximations for the periods of free modes can be made for these basins.

Equations (1.2) and (1.3) represent the free barotropic response of the lake with neither damping nor forcing considered. As mentioned at the beginning of this section, there are many potential excitation mechanisms for barotropic seiching. Some of these can be expressed as additional terms in Equation (1.2). A derivation of this equation from the basic equations of motion and continuity gives rise to terms that represent two forcing mechanisms: wind shear on the lake surface, τ_s, and atmospheric pressure deviations, p_a (Wilson, 1972). If damping is assumed to act linearly with damping coefficient K (e.g. Defant, 1960), then the governing equation for the depth-integrated velocity becomes:

$$\frac{\partial^2 q}{\partial t^2} + K\frac{\partial q}{\partial x} - gH(x)\frac{\partial^2 q}{\partial x^2} = F_s(x,t) \tag{1.4}$$

where the forcing term,

$$F_s(x,t) = \frac{1}{\rho}\left(\tau_s - H\frac{\partial p_a}{\partial x}\right).$$

Equation (1.4) reduces to Equation (1.2) for $K = F_s = 0$. In the case of a basin of uniform depth, the free solutions (i.e. $F_s = 0$) to Equation (1.4) are given by

$$q = Ae^{-Kt/2}\sin(kx)\sin(\gamma t + \epsilon),$$

where the resonant frequencies are

$$\gamma_n = \omega_n \sqrt{1 - \frac{K}{2\omega_n}}$$

and $\omega_n = k_n c = n\pi c L^{-1}$, $n \in \mathbb{Z}^+$, with the wave speed $c = \sqrt{gH}$. In the undamped case ($K = 0$), then $\gamma = \omega$ and the modal periods $T = 2\pi\gamma^{-1}$ are consistent with Merian's formula. In real basins, $K \neq 0$, but damping of barotropic seiching is typically small (Defant, 1960, Table 25) and the modal frequencies obtained by solving the free case (Equation 1.2) provide reasonable estimates of the damped frequencies, i.e. $\gamma \approx \omega$.

For a broader account of the subject of barotropic seiching, readers are directed to the work of Wilson (1972) who provides a thorough summary on the history of the subject as well as providing a great deal of detail on the relevant mathematics (including the derivation of Equation 1.4 from the equations of motion, and a full treatment of the forcing term F_s for atmospheric pressure disturbances). While now more than a century old, Chrystal (1905) similarly provides a summary of early works on the subject dating as far back as 1755, including a very thorough annotated bibliography containing 136 separate entries.

Baroclinic seiches

In addition to studying oscillations of the free surface of lakes, the early studies by the Scottish Lake Survey found evidence that the internal temperature field of Loch Ness also exhibits periodic motions (Murray, 1888). Watson (1904) recognized these oscillations as seiching of the interface between the epilimnion and hypolimnion and interpreted the forcing mechanism as an internal reaction to a surface wind shear. Due to their added complexity, their increased likeliness to exhibit non-linear behaviour, and their arguably greater importance compared to barotropic seiching, these baroclinic motions dominate modern literature in the subject of wind-induced oscillatory motion in lakes. Nonetheless, the present study will largely focus on barotropic rather than baroclinic seiching. As such, this section will only present one major result: the decoupling of vertical modes.

While a number of authors worked to build a mathematical framework for baroclinic seiching (e.g. Aichi, 1918a,b; Priestley, 1909; Wedderburn and Williams, 1911), major advances were made by Longuet-Higgins (1952) and Heaps and Ramsbottom (1966). In particular, Longuet-Higgins (1952) developed linearised equations for the free oscillations of deflections of both the water surface and the interface between density layers by starting from the

basic equations of motion and continuity. His work showed that as a result of the small density differences between layers ($\Delta\rho\rho_2^{-1} \sim O(10^{-3})$), barotropic and baroclinic motions can be effectively separated. The barotropic modes then respond as the modes of the equivalent homogeneous body of water, whereas for a two-layered system the interface deflection of the baroclinic modes ($\eta_n^{(2)}$) is given by

$$\eta_n^{(2)} = \cos(k_n x)[A_n \cos(\omega_n^{(2)} t) + B_n \sin(\omega_n^{(2)} t)]$$

where $\omega_n^{(2)} = k_n c^{(2)} = n\pi c^{(2)} L^{-1}$, $n \in \mathbb{Z}$, and the baroclinic wave speed $c^{(2)}$ is

$$c^{(2)} = \sqrt{g' \left(\frac{H_1 H_2}{H_1 + H_2} \right)}. \tag{1.5}$$

The gravitational restoring force acts on density differences, so the wave speed of internal modes depends on the "reduced gravity", g', which is expressed in terms of the upper and lower layer densities $\rho_{1,2}$:

$$g' = g \left(\frac{\rho_2 - \rho_1}{\rho_2} \right).$$

Longuet-Higgin's results produce a formula for modal periods analogous to Equation (1.1), and consistent with the one suggested by Watson (1904) much earlier.

Compared with barotropic motions, the reduced gravity of baroclinic modes results in these motions having amplitudes and periods that are typically 2 to 3 orders of magnitude greater than barotropic modes. For a sharp interface between layers, the two-layer circulation created by baroclinic motions (Figure 1.1b) leads to the generation of considerable shear between layers. This shear can act to dampen the baroclinic response (e.g. Horn et al., 2001; Imam, 2012; Imam et al., 2013b, 2017), or can lead to the growth of features such as Kelvin-Helmholtz instabilities or non-linear bores (Horn et al., 2001).

Longuet-Higgins (1952) actually considered a three-layered medium and showed a total of three "vertical" modes (one set of surface modes, and one set of modes for each of the two density interfaces). In general, the number of vertical modes present in a model will correspond to the number of density layers considered, with a theoretical infinite number of modes for a continuously stratified water column. Provided the effects of the Earth's rotation are unimportant and ignoring damping, the interface deflection of

the i^{th} vertical mode ($h^{(i)}$) is governed by

$$\frac{\partial^2 h^{(i)}}{\partial t^2} = \left[c^{(i)}\right]^2 \frac{\partial^2 h^{(i)}}{\partial x^2}$$

where $c^{(i)}$ is the wave speed of the corresponding mode (e.g. $c^{(2)}$ given by Equation (1.5)), and in the form presented here $c^{(i)}$ is independent of x. Considering that the barotropic wave speed $c^{(0)} = \sqrt{gH}$, this formula is consistent with Equation (1.3).

Imam (2012, Chapter 1) provides more detailed review of the baroclinic seiche process, and the variety of models (analytical and numerical) that have been developed to consider both free and forced responses.

Effects of the Earth's rotational

For basins that are large enough or of high enough latitude, the rotation of the Earth becomes important. This is reflected in the addition a Coriolis term in the equations of motions. Csanady (1975) provides a detailed review on the modifications this term has on the seiche response of the lake. The importance of this term to the surface/internal seiche can be determined by considering the external/internal Rossby radius of deformation,

$$R = \frac{c}{f}, \tag{1.6}$$

where c is the wave speed of either barotropic or baroclinic waves, and f is the Coriolis parameter, and comparing it to the transverse horizontal length scale of the lake. If R is much larger than the lateral horizontal scale of the basin then rotational effects are unimportant, whereas if it is much smaller then rotational effects dominate the response.

In the classification of lakes that this study considers (fjord-type lakes), rotational effects are typically unimportant for barotropic seiching and while they may play a role in the baroclinic response, they rarely dominate that response. With this in mind, no further review of this subject is presented.

1.2.2 Influence of complex geometry on seiching

The simplicity of the geometry of the Scottish Lochs allowed for studies that provided a great deal of insight into the relevant mechanisms of both barotropic and baroclinic seiching. Of course, many basins don't conform to the geometric constraints of narrow, elongated lakes devoid of islands, bays, sub-basins, or multiple arms. In most cases, studies of complex lakes

occur on a case-by-case basis and so it is difficult to make generalizations about the impact of specific geometric features unless many studies have been completed. A body of literature exists regarding the seiche response of lakes with multiple basins that are separated by shallow sills or constrictions (e.g. Appt et al., 2004; Dorostkar and Boegman, 2013; Farmer, 1978; Imam et al., 2013a; Laval et al., 2008; Van Senden and Imboden, 1989), and so some general concepts are understood in those geometries. Theory also exists for seiching in small bays and harbours of large lakes (e.g. Schwab and Rao, 1977; Wilson, 1972), but rarely are these considered in conjunction with the response of the whole lake (Kirillin et al., 2014, provides a notable exception). For other geometric features such as islands or multiple arms, far fewer studies exist.

The lack of literature concerning seiching in multi-armed lakes may be due in part to the added difficulty in providing a full explanation for the spatial variability of the observed periods combined with the need to employ some form of numerical solver to determine both periods and mode-shapes. Malinina and Solntseva (1972, as cited in Rudnev et al., 1995), among others, attempted to explain the barotropic periodicities observed in Lake Onega by applying Merian's formula along some extent of the lake; however, as explained by Rudnev et al. (1995), this methodology incorrectly predicts higher modes and fails to explain periodicities that seem to occur only in specific arms. To fully describe this response, Rudnev employed a numerical method to solve the 2-dimensional depth-varying wave equations (see Section 1.2.3 below for more details). Numerical solvers are the norm for predicting seiche modes in multi-armed geometries. Similar techniques to those employed by Rudnev were used to study barotropic seiching in Lake Como by Buzzi et al. (1997), and later baroclinic seiching in the same lake by Guyennon et al. (2014). Carter and Lane (1996) applied a similar method in a few New Zealand Lakes, including multi-armed lake Te Anua. In a study of multi-armed Clear Lake, (Rueda and Schladow, 2002) present the relevant mathematics behind this method as applied on an unstructured grid, and in an online supplement provide their code for download; however, in studying internal wave dynamics, the same authors instead employed a fully 3-dimensional hydrodynamic model (Rueda and Schladow, 2003). A 3-dimensional hydrodynamic model was similarly employed in a study of wind-forced baroclinic waves in two basins of Nechako Reservoir (Imam, 2012; Imam et al., 2017), though based on only the longest extent of the lake, a semi-analytical model also produced favourable results (Imam et al., 2013b). A two-dimensional, non-linear, forced model was applied to understand the seiche response to seismic activity in "Y"-shaped Lake Union (Barberopoulou,

2008). Of the multi-armed lakes mentioned, only in Lake Como (Buzzi et al., 1997; Guyennon et al., 2014) and Nechako Reservoir (Imam, 2012; Imam et al., 2017) is characterization of mode periods and shapes for the fjord-like morphotype of interest given, and no relevant results were found with analytical methods.

Based on these few studies, little can be said about the general response of multi-armed lakes. One interesting behaviour is evident in lakes with complex geometries when wave modes are developed in a 2-dimensional domain: many of these lakes have modes that are localized to individual bays or arms of a lake. In Flathead lake, where subsections of the lake are distinct bays, a hydrodynamic model applied to the whole lake finds modes that act as bay-modes with modal periods close to those predicted using an open-mouthed application of Merian's formula (Kirillin et al., 2014). In Lake Onega many higher modes act primarily within a single arm, with near-zero deflections of the surface in the remainder of the lake (Rudnev et al., 1995); however, in this lake, the distinction between "arms" and "bays" is unclear, and these modes may be more in line with those predicted by (Kirillin et al., 2014). Lake Como is distinctly multi-armed, and both the barotropic and baroclinic responses show an exaggerated form of this behaviour: the second horizontal mode has one arm that is essentially decoupled from the other two (Buzzi et al., 1997; Guyennon et al., 2014). However, multi-armed Natalkuz Lake does not show a similar behaviour (Imam, 2012; Imam et al., 2017).

Neumann (1944, as cited in Defant, 1960) developed a method for studying interconnected basins using the concept of impedance borrowed from the study of electrical circuits. In this method, the impedance of a system is defined as

$$Z = \frac{\text{amplitude of pressure}}{\text{area} \times \text{amplitude of velocity}},$$

and the modal frequencies are found by minimizing the impedance Z. For an undamped system, this minimum is $Z = 0$. To account for the separate basins, each basin is assigned an impedance factor, Z_i based on its connections to other basins. For example, for a basin open at both ends,

$$Z = \frac{i\rho c}{A} \tan\left(\frac{\omega L}{c}\right),$$

and for a basin closed at one end

$$Z = \frac{i\rho c}{A} \cot\left(\frac{\omega L}{c}\right).$$

These impedances are added using rules similar to adding the resistors in electrical circuits. For basins configured in series, $S = \sum Z_i$, for those

configured in parallel, $P^{-1} = \sum Z_i^{-1}$. Then total resistance Z is the sum of all basins connected in parallel or series. Both Wilson (1972) and Defant (1960) show examples of this method being applied to both fully and semi-enclosed basins with branched arms. This method provides perhaps the only methodology for predicting the seiche periods of a multi-armed lake without using a numerical technique. However, despite the potential usefulness of this method, this author has been unable to find any example of it being applied to a multi-armed lake. Furthermore, as will be discussed in Chapter 2, the impedance method is unable to predict certain features of the response.

1.2.3 Finite Element Method for solving the wave equation in an arbitrary two-dimensional domain

Given the prevalence of this technique and also due to it's employment in Chapter 3 of this thesis, I will briefly describe the development of a Galerkin-type Finite Element Method (FEM) numerical technique. Specifically, this section will describe the use of this technique on an unstructured grid. This can be seen as a summary of Rueda and Schladow (2002), though the use of this technique in describing seiche modes in lakes pre-dates that publication (e.g Carter and Lane, 1996; Hutter et al., 1982).

In an arbitrary shaped 2-dimensional domain Ω with boundary $\partial\Omega$, Equation (1.3) and the "no-flow" boundary condition become

$$\nabla \cdot (H\nabla\eta) + \left(\frac{\omega^2}{g}\right)\eta = 0, \text{with} \tag{1.7a}$$

$$\nabla\eta \cdot \hat{\boldsymbol{n}} = 0 \text{ on } \partial\Omega, \tag{1.7b}$$

where the operator ∇ is defined in along the two horizontal dimensions: $\nabla = (\partial_x, \partial_y)$, and $\hat{\boldsymbol{n}}$ is the outward unit normal vector on $\partial\Omega$.

For simplicity, let $\Lambda = \omega^2 g^{-1}$. Then the weak formulation of Equation (1.7) is attained by multiplying Equation (1.7a) by a test function ψ, integrating over Ω, expanding with Green's first identity, and using Equation (1.7b) to eliminate boundary terms. The result is

$$-\int_\Omega (\nabla\psi)\cdot(H\nabla\eta)\,dA + \Lambda\int_\Omega \psi\eta dA = 0. \tag{1.8}$$

While Equation (1.8) is still exact, it is referred to as the weak form of Equation (1.7) because it only satisfies the equation in an integral sense. While any solution of Equation (1.7) will satisfy Equation (1.8), the reverse is not true. To ensure that solutions to Equation (1.8) satisfy Equation (1.7),

we need to satisfy Equation (1.8) with $\psi(x, y) = \delta(x, y)$ for every $(x, y) \in \Omega$ (which is an infinite number of test functions).

The standard Galerkin procedure is to discretize Equation (1.8) onto the finite dimensional subspace S_n of dimension N. In particular, we consider a subspace S_n that can be described by an unstructured triangular mesh. Then each set of (x, y) coordinates maps to a single numbered node n (see Figure 1.2). In this discrete space, the continuous function $\eta(x, y)$ is approximated by $\tilde{\eta}(x_n, y_n)$. If the set of basis functions $\{\Psi_j(x, y)\}_{j=1}^{N}$ span S_n where N is the total number of nodes in S_n, then $\tilde{\eta}$ can be represented as a linear combination of those basis functions:

$$\tilde{\eta}(x_j, y_j) = \sum_{j}^{N} \tilde{\eta_j} \Psi_j.$$

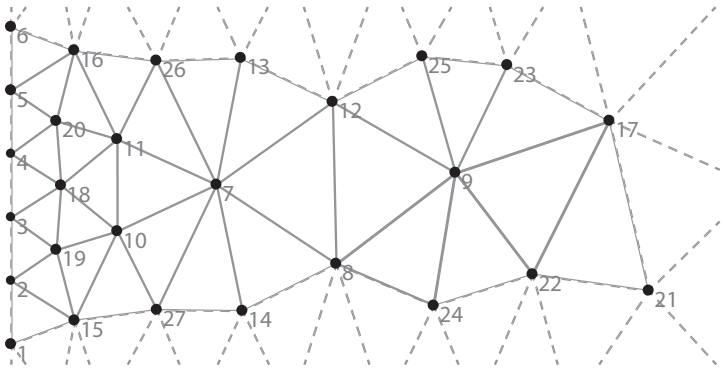

Figure 1.2: Schematic of the type of unstructured triangular mesh used in the FEM analysis. Each set of (x, y) coordinates at each node is defined by a single number n.

By choosing appropriate functions in the discrete subspace for the test functions ψ, the the solution to Equation (1.7) on the continuous domain Ω is approximated on a discrete domain by the matrix problem

$$\mathbf{K}\tilde{\eta} = \Lambda \mathbf{M}$$

where the matrices $\mathbf{K}$ and $\mathbf{M}$, called the "stiffness" and "mass" matrices respectively. Taking the basis functions for the test functions $\psi = \Psi_i$, these matrices are given by

$$K_{ij} = \int_{\Omega} H(\nabla \Psi_i)(\nabla \Psi_j) dA,$$

$$M_{ij} = \int_{\Omega} \Psi_i \Psi_j dA,$$

and are dimension $N \times N$. In the simplest case, the basis functions are the "pyramids":

$$\Psi_k(x_l, y_l) = \begin{cases} 1 & \text{if } k = l \\ 0 & \text{if } k \neq l \end{cases} \qquad k, l = 1, \ldots, N.$$

Then the matrices $\mathbf{K}$ and $\mathbf{M}$ can be constructed using simple geometric arguments (e.g. Alberty et al., 1999).

The eigenvalues Λ of the original problem are then the eigenvalues of the matrix $\mathbf{M}^{-1}\mathbf{K}$, and the modeshapes are given by the corresponding eigenvectors. In general, both $\mathbf{M}$ and $\mathbf{K}$ will be sparse, and a number of techniques exist for approximating the eigenvalues of $\mathbf{M}^{-1}\mathbf{K}$, such as the Lanczos procedure (Schwab, 1980). Some modern computer programs, such as *Matlab* have inbuilt solvers for this (in *Matlab*, the eigenvalues of this matrix can by found by using the `eigs` function).

1.3 Objectives and organization

This study examines the impact of surface geometry of a lake on the expected modes of the free oscillatory response. In particular, focus is placed on fjord-type multi-armed lakes. Fjord-type lakes are typically elongate and narrow, so considering this classification of lakes allows for the study to address the importance of multiple arms without having to address additional complexities associated with rotational effects or interactions with transverse modes. Rather than present a single case, the study attempts to make general statements about the impact of this geometric feature.

The remainder of this document is organized as follows:

Chapter 2 takes a theoretical approach to develop a simplified analytical model that can predict mode shapes and periods for standing waves in multi-armed lakes with an arbitrary number of arms. The implication of model parameters on the solution space is discussed.

Through a combination of observations and modelling, Chapter 3 describes the barotropic seiche response of two multi-armed lakes of similar geometry. Both Quesnel Lake (located in British Columbia, Canada) and Lake Como (located in the Lombardy region of Italy) are "Y"-shaped fjord-type lakes. By comparing the responses of these two lakes, further insight is gained into the impact of this geometric feature. The analytical model discussed in Chapter 2 is considered in the context of these lakes.

Chapter 2

Development of an analytical solution for seiche modes in fjord-type multi-armed lakes

2.1 Introduction

Despite the broad analytical work in the subjects of both barotropic and baroclinic seiching done by oceanographers and limnologists studying simple lakes (e.g. Chrystal, 1905; Defant, 1960; Longuet-Higgins, 1952; Wedderburn and Williams, 1911), the application of their techniques to more complex geometries has required the use of numerical techniques (e.g. Rudnev et al., 1995; Schwab and Rao, 1977). While these numerical solvers are valuable tools and may be simple to use (Rueda and Schladow, 2002), they must still be applied on a case-by-case basis. Thus, in order to understand the behaviour inherent in a particular geometric feature, a wide enough body of literature needs to be established to make inferences from those results. Because many types of geometric complexity are fundamentally two-dimensional features (e.g. constrictions, bays, or multiple arms), it is difficult to approach these problems using an analytical framework.

This chapter focuses on the development of a simplified analytical model for predicting the free mode periods and mode shapes for fjord-type multi-armed lakes. The model will consider only the defining geometric consideration of these lakes: their multi-armed nature. The oscillatory response of real lakes will be modified by many factors; by removing all of these complexities except the fundamental geometric feature, understanding can be gained about which behaviours can be attributed the interaction of the arms of the lake.

2.2 Model Development

2.2.1 Governing equations

We consider the linearised equations of motion and continuity for a hydrostatic, homogeneous fluid, ignoring the Coriolis terms, frictional effects, and external forcing. Further, motion is assumed to primarily along the longitudinal axis of the lake, so transverse motions are neglected. Then the equations of motions are:

$$\text{Momentum:} \qquad \frac{\partial q}{\partial t} + gH\frac{\partial h}{\partial x} = 0 \tag{2.1a}$$

$$\text{Continuity:} \qquad \frac{\partial h}{\partial t} + \frac{\partial q}{\partial x} = 0 \tag{2.1b}$$

where $H(x)$ is the still water depth, $h(x,t)$ is the surface deflection (the total depth is given by $H+h$), and $q(x,t)$ is the depth-integrated horizontal velocity ($q = \int_0^H u dz$). To arrive at these we have assumed a constant width $b(x) = b$ and that deflections are small compared to total depth $h(x,t) \ll H(x)$. Moving forward, it will be useful to non-dimensionalize x and $H(x)$ as follows:

$$x^* = \frac{x}{L} \qquad H^* = \frac{H(x)}{H_0}$$

In general we will consider these equations within the domain $x \in [0, L]$, so $x^* \in [0, 1]$. H_0 is some characteristic depth so H^* is $O(1)$.

Making these substitutions, we combine Equations (2.1a) and (2.1b) and assume an oscillatory response $q(x,t) = \phi(x)e^{i\omega t}$, and $h(x,t) = \eta(x)e^{i\omega t}$. This results in two ordinary differential equations for the mode shapes:

$$\frac{d}{dx^*}\left(H^*\frac{d\eta}{dx^*}\right) + \lambda^2\eta = 0, \tag{2.2a}$$

$$H^*\frac{d^2\phi}{dx^{*2}} + \lambda^2\phi = 0 \tag{2.2b}$$

where the non-dimensional eigenvalue λ is given by $\lambda = \omega L(gH_0)^{-1/2}$. It will be convenient to define a parameter, called "wave travel time", as $\tau = L(gH_0)^{-1/2}$, so $\lambda = \omega\tau$.

From Equations (2.1a) and (2.1b) we have that the mode shapes η and ϕ are related by

$$\phi = i\left(\frac{\sqrt{gH_0}}{\lambda}\right)H^*\frac{d\eta}{dx^*}, \qquad \text{and} \qquad \eta = i\left(\frac{1}{\lambda\sqrt{gH_0}}\right)\frac{d\phi}{dx^*} \tag{2.3}$$

where the inclusion of the imaginary number $i = \sqrt{-1}$ simply indicates that h and q are 90^o out of phase in time.

Sturm-Liouville Boundary Value Problems

Before considering the solutions, it will be useful to place Equations (2.2a) and (2.2b) in the context of a broader mathematical theory which allow us to mention some known properties of these equations. Through the early 19th century, a number of advances were made in understanding a classification of boundary value problems that often arise in when considering separable PDEs. These problems are now called "Sturm-Liouville" (SL) problems (Boyce and DiPrima, 1986) and have the form

$$\frac{d}{dx}\left[p(x)\frac{dy}{dx}\right] + [\lambda w(x) - q(x)]y = 0 \tag{2.4}$$

over the finite interval [a,b] together with the boundary conditions

$$\alpha_1 y(a) + \alpha_2 \frac{dy}{dx}(a) = 0 \tag{2.5a}$$

$$\beta_1 y(b) + \beta_2 \frac{dy}{dx}(b) = 0 \tag{2.5b}$$

for some prescribed constants α_1, α_2, β_1, β_2. The theory also requires that

$$p(x), w(x) > 0 \text{ on } (a,b), \quad p^{-1}, q, w \in L^1_{\text{loc}}([a,b])$$

In these equations, non-null solutions are only allowed for certain discrete values of the parameter λ. These eigenvalues, λ_n, are found by solving

$$\Pi(\lambda) = 0$$

Where $\Pi(\lambda)$ is the equation obtained by substituting the general solution to Equations (2.4) and (2.5a) into Equation (2.5b). If $Y(x,\lambda)$ solves Equations (2.4) and (2.5a), then

$$\Pi(\lambda) = -\left(\frac{\beta_2}{\beta_1}\right)\left(\frac{1}{Y(b,\lambda)}\frac{dY}{dx}(b,\lambda)\right)$$

The central theorem of Sturm's first memoir (Everitt, 2005; Hinton, 2005) gives that

$$\frac{d}{d\lambda}\left(\frac{p}{y}\frac{dy}{dx}\right)(x,\lambda) < 0 \tag{2.6}$$

where y is a solution to Equations (2.4), (2.5a) and (2.5b).And so

$$\text{sign}\left(\frac{d\Pi}{d\lambda}\right) = -\text{sign}\left(\frac{\beta_2}{\beta_1}\right).$$

Following from this, the theorem predicts the following two properties of SL equations that we will make use of.

1. Eigenvalues are real and form an infinite sequence of increasing magnitude:
$$\lambda_1 < \lambda_2 < \ldots < \lambda_n < \ldots \to +\infty$$

2. Eigenvalues are simple. That is, for each eigenvalue λ_n, there is a single, unique (up to a constant), eigenfunction y_n that satisfies Equation (2.4). These functions can be written as
$$y_n(x) = A_n y(x, \lambda_n)$$
for some mode-dependant constant A_n.

A great number of other properties of these equations are also known (for a list of theorems see Hinton, 2005), but these will not be invoked in the present study.

2.2.2 Description of the multi-armed model

While there are a number of different geometries that can fall under the description of "multi-armed lakes", we consider the case of N arms radiating outward like spokes from one central confluence point. To solve for the wave response, a coordinate system is set up in each arm such that the local x-axis, x_i^*, coincides with that arm's primary longitudinal direction. Some of the algebra will be simplified by using a coordinate system with positive x_i^* moving inwards towards the confluence (see Figure 2.1). Thus, the two-dimensional domain is converted to a set of N coupled one-dimensional domains, and Equations (2.2a) and (2.2b) are used to predict the longitudinal variation in η_i and ϕ_i along each arm.

Equations (2.2a,b) are applied in each arm with boundary conditions applied at the endpoints $x_i^* = 0, 1$ as follows:

BC1: $\phi_i(0) = 0$ (i.e. no flow condition),

BC2: $\eta_i(1) = \xi_i$, and

BC3: $\phi_i(1) = \sigma_i$,

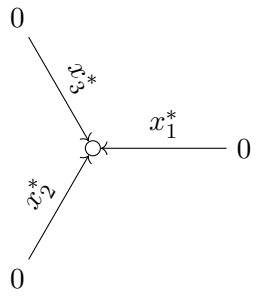

Figure 2.1: Schematic representation and coordinate definitions of the multi-armed system being considered in the present study for the case $N = 3$.

where ξ_i and σ_i are prescribed constants (however, the values of these constants will be found through the coupling procedure discussed below rather than strictly prescribed). Making use of Equation (2.3) allows the combination of BC2 and BC3 into a boundary condition in SL form:

$$\xi_i \phi_i(1) + \left(\frac{\sigma_i}{\lambda \sqrt{g H_{0,i}}} \right) \frac{d\phi_i}{dx_i^*}(1) = 0. \tag{2.7}$$

A similar result can be shown for η_i. Here, the eigenparameter λ exists in the boundary conditions, along with σ_i and ξ_i which will be shown to both be mode-dependant values. While this is not necessarily consistent with classic SL problems, Schneider (1974) has shown that the relevant SL properties still hold.

The set of N ODEs is coupled at the junction by imposing conditions on ξ_i and σ_i. Strictly, these conditions act as a set of boundary conditions on Equations (2.1a) and (2.1b), but we will refer to them separately as "coupling conditions". They are given as follows:

CC1: Continuity of surface height: $\xi_1 = \xi_2 = \ldots = \xi_N$

CC1: Conservation of mass: $\sum_{i=1}^{N} b_i \sigma_i = 0$

for b_i the width of the i^{th} arm at the junction. For simplicity, for the remainder of this document we will assume $b_1 = b_2 = \ldots = b_N$, and so drop the b_i from this condition

CC1: Preservation of these properties through time: $\omega_{1,n} = \omega_{2,n} = \ldots = \omega_{N,n}$

.

Within each arm, the solutions to Equations (2.2a,b) depend on the form of H^*. Nonetheless, the conditions necessary to couple the equations can be

applied for the general form and thus the derived solutions and behaviour become largely independent of the actual form of H^*.

We take advantage of the SL property (2) that eigenfunctions are simple and write the eigenfunctions for each mode, n, and arm, i, as

$$\eta_{i,n} = A_{i,n}\eta(x_i^*, \lambda_{i,n})$$
$$\phi_{i,n} = \alpha_{i,n}\phi(x_i^*, \lambda_{i,n})$$

where the functions $\eta(x_i^*, \lambda_{i,n})$ and $\phi(x_i^*, \lambda_{i,n})$ are known, and determined by satisfying Equations (2.2a) and (2.2b) together with **BC1**, and $A_{i,n}$ and $\alpha_{i,n}$ are some mode dependant constants for each arm that are yet to be determined. These constants will be linearly related through Equation (2.3), so $\alpha_{i,n} = C_i A_{i,n}$, where C_i are also known. In general C_i depend on the form of H^*, but for all the situations considered in the present study, $C_i = \sqrt{gH_{0,i}}$.

To apply **BC2**, we set the value of $\eta_{i,n}$ at the confluence to be equal to the defined constant ξ_i, so $\xi_i = A_{i,n}\eta(1, \lambda_n)$. To proceed, it is necessary to consider two cases for ξ_i: either $\xi_i \neq 0$ or $\xi_i = 0$. As we will show immediately, the former condition allows for the mode shapes to be determined with ease, but creates a more complicated expression to determine the frequencies. In the latter case, the expression for ω_n is straightforward, but more effort must be applied to arrive at the mode shapes.

Case 1: $\xi_i \neq 0$

For the case where $\xi_i \neq 0$, **BC2** can be rearranged to give $A_{i,n}$ in terms of ξ_i. Because $A_{i,n}$ is a mode dependant constant based on initial conditions, ξ_i is also mode dependant: $\xi_i = \xi_{i,n}$. Furthermore, the application of **CC1** indicates that $\xi_{i,n}$ is independent of which arm it is being applied to: $\xi_{i,n} = \xi_n$. Thus, we obtain the following expressions for η and ϕ:

$$\eta_{i,n}(x_i^*) = \xi_n \frac{\eta(x_i^*, \lambda_{i,n})}{\eta(1, \lambda_{i,n})},$$
$$\phi_{i,n}(x_i^*) = \xi_n C_i \frac{\phi(x_i^*, \lambda_{i,n})}{\eta(1, \lambda_{i,n})}.$$

Then **BC3** gives:

$$\sigma_i = \xi_n C_i \frac{\phi(1, \lambda_{i,n})}{\eta(1, \lambda_{i,n})}. \tag{2.9}$$

The values $\lambda_{i,n}$ can be determined by solving this equation if ξ_n and σ_i are prescribed. However, these values are not prescribed but instead given by

imposing the "coupling conditions". Substituting Equation (2.9) in **CC2**, and factoring out ξ_n yields

$$f(\omega_n) = \sum_{i=1}^{N} C_i \frac{\phi(1, \omega_n \tau_i)}{\eta(1, \omega_n \tau_i)} = 0. \tag{2.10}$$

If $\tau_1 \neq \tau_2 \neq \ldots \neq \tau_N$ (denoted the TNE case), the modal frequencies ω_n are found by finding values of ω that satisfy $f(\omega) = 0$. However, if $\tau_i = \text{constant} = \tau$ (denoted the TE case), Equation (2.10) simplifies to

$$f(\omega_n) = \phi(1, \omega_n \tau) = 0$$

If z_n^{ϕ} are the roots of $\phi(1, z)$, then the modal frequencies ω_n are given by $\omega_n = z_n^{\phi} \tau^{-1}$.

Case 2: $\xi_i = 0$

In the second case that $\xi_i = \xi_n = 0$, **BC2** demands that $A_{i,n}\eta(1, \lambda_{i,n}) = 0$, so to avoid trivial solutions, we require that $\eta(1, \lambda_{i,n}) = 0$. The results presented for $\xi_i \neq 0$ would thus imply division by zero and are invalid. Instead, if z_n^{η} are the roots of $\eta(1, z)$, then ω_n are given simply by $\omega_n = z_n^{\eta} \tau_i^{-1}$. However, if τ_i conform to the TNE case ($\tau_1 \neq \tau_2 \neq \ldots \neq \tau_N$), then this will produce different frequencies for each arm. In order to satisfy Equations (2.1a,b) for all time, ω_n must be equal for all arms (**CC3**). This indicates that ξ_n cannot equal zero except in the TE scenario that $\tau_i = \text{constant}$.

Then **BC3** gives $\sigma_{i,n} = \alpha_{i,n}\phi(1, z_n^{\eta})$. Recognizing that $\phi(1, z_n^{\eta})$ are equal across all arms and can be factored out, **CC2** is reduces to

$$\sum_{i=1}^{N} \alpha_{i,n} = 0.$$

There are an infinite number of values of $\alpha_{i,n}$ that satisfy this condition, but if we separate $\alpha_{i,n}$ into a mode-dependent component, ζ_n, and an arm-dependent component, γ_i, so that $\alpha_{i,n} = \zeta_n \gamma_i$, then we can construct γ_i so that it forms a basis. For γ_i given by

$$\gamma_i = \begin{cases} 1 & \text{if } i = j \text{ and } i \neq k \\ -1 & \text{if } i = k \\ 0 & \text{otherwise} \end{cases}$$
$$j = 1, \ldots, (N-1)$$
$$k = (j+1), \ldots, N$$

then all $\alpha_{i,n}$ can be expressed as a linear combination of $\zeta_n\gamma_i$, and **CC2** is satisfied. Then equations $\eta_{i,n}$ and $\phi_{i,n}$ are given by

$$\eta_{i,n}(x_i^*) = \frac{\zeta_n\gamma_i}{C_i}\frac{\eta(x_i^*, z_n^\eta)}{\phi(1, z_n^\eta)} \tag{2.11a}$$

$$\phi_{i,n}(x_i^*) = \zeta_n\gamma_i\frac{\phi(x_i^*, z_n^\eta)}{\phi(1, z_n^\eta)} \tag{2.11b}$$

Physically, the values of γ_i indicate that in these modes all the flow exiting one arm will enter exactly one different arm (for each mode, exactly 2 arms will be active all the others will be quiescent). Here, each eigenvalue is repeated with multiplicity given by the number of possible combinations of γ_i, which is given by the binomial coefficient ${}_NC_2$ (i.e. for a three armed lake, eigenvalues will have multiplicity ${}_3C_2 = 3$; for a four armed lake, eigenvalues will have multiplicity ${}_4C_2 = 6$; etc.). This presents difficulties in determining the values ζ_n; in order to solve for these values using the initial conditions, the values of γ_i will need to be specified. Without this specified, there may be no unique solution for ζ_n. Indeed, this set of basis functions are not uniquely defined and other bases can also produce viable results; however, if another set of basis functions was specified then a linear combination of those functions would yield eigenfunctions that match the current choice and so this decoupled response is not an artefact of the choices made here.

If Equation (2.10) is naively used when the wave travel times for each arm are equal, then the z_n^η wave modes and their repetitions will be missed. Thus, having $\tau_i = \text{constant}$ leads to two separate equations that define ω_n:

$$\omega_n = \frac{z_n^\eta}{\tau} \tag{2.12a}$$

$$\omega_m = \frac{z_m^\phi}{\tau}. \tag{2.12b}$$

Equation (2.12a) corresponds to a node existing at the confluence (and has the multiplicity discussed above), and Equation (2.12b) corresponds to a anti-node existing at the confluence (and has no multiplicity). As a result of the first SL property, the function $\eta(1, \lambda)$ is oscillatory in λ and will have an infinite number of roots. Sturm's oscillation theorem then gives that the roots of $\frac{d\eta(1,\lambda)}{d\lambda}$ will occur between subsequent roots of η (Boyce and DiPrima, 1986). By using Equation (2.3) it can be shown that for the geometries considered in Section 2.2.4, $\phi(1, \lambda) \propto \frac{d\eta(1,\lambda)}{d\lambda}$, so the roots z_m^ϕ will occur between subsequent values of z_n^η (e.g. $z_1^\eta < z_1^\phi < z_2^\eta$), and $z_n^\eta \neq z_m^\phi$ for all m, n.

Following the methods described in this section, it can be shown that the mixed case (denoted TM) where there are a total of M arms with the same value of τ_i (i.e. $\tau_i = \tau_{i+1} = \ldots = \tau_M$), but M is fewer than the total number of arms ($1 < M < N$), then there will be a repetition of the eigenvalues associated with only those arms with equal values of τ_i, and so eigenvalues that correspond to $\omega_n = z_n^\eta \tau_M^{-1}$ will have multiplicity of ${}_MC_2$, and all other eigenvalues will have multiplicity 1. To calculate the full set frequencies ω_n of the TM case, it is necessary to take both the frequencies predicted by Equation (2.10), and an additional set of frequencies predicted using Equation (2.12a) with $\tau = \tau_M$. As before, the set of frequencies calculated with Equation (2.12a) will be those that exhibit decoupled behaviour.

2.2.3 Alternate method for calculating ω_n

In the case that τ_i = constant, the modal frequencies ω_n are determined simply by $\omega = \{z_n^\eta \tau^{-1}, z_n^\phi \tau^{-1}\}$, $n \in \mathbb{Z}^+$. When $\tau_i \neq$ constant, there is no closed form solution for ω_n but the values z_n^η still have a bearing on the solution. When $\omega_n \tau_i = z_n^\eta$, then the function $\eta(1, \lambda_{i,n}) = 0$. Because this appears in the denominator of Equation (2.10), any time $\omega_n \tau_i \to z_n^{\eta\pm}$ then $f(\omega) \to \pm\infty$. By using Equation (2.6), it can be shown that

$$\frac{d}{d\omega} f(\omega) > 0.$$

So between each set of asymptotes, there will be a single root of $f(\omega)$.

Consider a sequence Ω constructed as

$$\Omega = \text{sort}\left(z_n^\eta {\tau_i}^{-1} : i = 1, \ldots N, n \in \mathbb{Z}^+\right)$$

where the operator *sort* arranges elements monotonically from smallest to largest, and the sequence retains repeated values. Then the values of Ω correspond to subsequent ω such that $f(\omega)$ diverges (i.e. Ω are the ordered sequence of asymptotes of $f(\omega)$). Then the values of ω_n are constrained by the values of Ω:

$$\Omega_n \leq \omega_n \leq \Omega_{n+1}.$$

In fact, this behaviour is retained in the case that τ_i = constant and in the TM case.

Because $f(\omega)$ diverges rapidly away from $\omega = \omega_n$, these modal frequencies can be approximated by

$$\omega_n \approx \frac{\Omega_n + \Omega_{n+1}}{2}. \tag{2.13}$$

The advantage to this methodology is that if $\tau_i = \tau_j$ (repetition of one or more values of τ), then for some n, we will have $\Omega_n = \Omega_{n+1} = z_n^{\eta}\tau_{(i,j)}^{-1}$, so the correct value of ω_n will be calculated. In addition, this method will yield the correct multiplicity of eigenvalues.

As will be discussed further in Sections 2.3.1 and 2.3.2, by considering this pattern, additional insight can be gained into response of the lake.

2.2.4 Solutions for analytically defined bottom profiles

The solution to Equations (2.2a) and (2.2b) depend on the form of H^*. For certain analytically defined bottom depth profiles these equations have functional solutions. The model developed here will be applied for the two simplest geometries of depth variation: a constant bottom profile ($H(x) = H_0$), and a linearly varying profile ($H(x) = (H_0/L)x$). Solutions can similarly be developed for a limited number of more complicated functions H^* (e.g. Chrystal (1905) considers a parabolic bottom profile[1]: $H(x) = H_0[1 - (2xL^{-1})^2]$).

The general solutions to Equations (2.2a) and (2.2b) for a constant bottom are given simply by trignometric functions:

$$\eta(x^*) = A\cos(\lambda x^*) + B\sin(\lambda x^*)$$
$$\phi(x^*) = \alpha\sin(\lambda x^*) + \beta\cos(\lambda x^*).$$

For linear bottom variation of the form $H(x) = (H_0/L)x$, a variable substitution $\chi = 2\lambda\sqrt{x^*}$ will convert Equation (2.2a) to Bessel's equation, so the functions η and ϕ are given in terms of Bessel functions:

$$\eta(x^*) = A\mathrm{J}_0\left(2\lambda\sqrt{x^*}\right) + B\mathrm{Y}_0\left(2\lambda\sqrt{x^*}\right)$$
$$\phi(x^*) = \alpha\sqrt{x^*}\mathrm{J}_1\left(2\lambda\sqrt{x^*}\right) + \beta\sqrt{x^*}\mathrm{Y}_1\left(2\lambda\sqrt{x^*}\right).$$

In order to satisfy **BC1** we require $B = \beta = 0$ for both cases of depth

[1] Chrystal (1905) solved Equation (2.2b) using a standard power series expansion of the form $\phi(\chi) = a_0 + a_1x + a_2x^2 + \ldots$, and found two linearly independent series solutions for ϕ which he named "Seiche-cosine" and "Seiche-sine". In this case, a transformation of Equation (2.2a) yields Legendre's equation, so a closed form solution exists in terms of Legendre Polynomials which are closely related to the functions Chrystal developed.

variation. Then Equation (2.10) becomes

$$\text{Constant Bottom:} \qquad \sum_{i=1}^{N} \sqrt{gH_{0,i}} \tan(\omega_n \tau_i) = 0, \tag{2.14}$$

$$\text{Linear Bottom:} \qquad \sum_{i=1}^{N} \sqrt{gH_{0,i}} \frac{J_1(2\omega_n \tau_i)}{J_0(2\omega_n \tau_i)} = 0, \tag{2.15}$$

2.2.5 Solutions for an arbitrary bottom profile

A general solution for the SL equation does not exist (Hinton, 2005). To solve Equations (2.2a) and (2.2b) for an arbitrary function H^* it is necessary to use some approximate approach. The most accurate approximate approach is the use of a numerical scheme which will produce solutions of arbitrarily high precision provided a small enough step size, but such an approach defeats the spirit of the present study and so it will not be employed here. Other methods of approximation include breaking the bathymetry into smaller sections which can each be fitted with an polynomial curve (Chrystal, 1905; Chrystal and Wedderburn, 1905), or the use of an asymptotic approach.

The WKB method is one such asymptotic approach appropriate for equations of this form. This approach gives approximate solutions to the equation

$$\frac{d^2y}{dx^2} + \lambda^2 f(x) y = 0$$

accurate for large eigenvalues, as $\lambda \to \infty^+$ (Bender and Orszag, 1999). While the approach is perhaps more popular in fields such as optics, it has nonetheless been applied to understanding the nature of water waves (LeBlond and Mysak, 1978), and in a theoretical framework has even been applied to the problem of seiches (Ortiz et al., 2013). The method is occasionally referred to as the Liouville-Green (LG) method for work that those mathematicians did in the 19$^{\text{th}}$ century; in fact, the work of Green (1837) in developing ideas associated with this approach involved wave propagation in an elongated channel with varying depth and width.

The WKB method assumes a solution of the form $y(x) \sim e^{\lambda S(x)}$ and, following the standard perturbation approach, $S(x)$ is expanded in an infinite series around a small parameter (chosen to be λ^{-1}):

$$S(x) = \sum_{n=0}^{\infty} \frac{1}{\lambda^n} S_n(x).$$

This expansion is substituted back into the original equation and the $S_0(x)$ and $S_1(x)$ terms are retained and computed. Then, if $f(x) > 0$ for all x the result is

$$y(x) \sim \frac{\alpha}{[f(x)]^{1/4}} \sin\left(\lambda \int^x \sqrt{f(s)} ds + \theta\right)$$

for arbitrary amplitude α and phase θ. This formula can be applied to Equation (2.2b) directly to find the asymptotic behaviour of ϕ. A leading order solution for η can be found by either applying Equation (2.3) to the result, or using a variable substitution $\eta = Y(x^*)(H^*)^{-1/2}$ in Equation (2.2a) and thus converting it to a form that the WKB approximation can be applied. Both methods produce the same result, but first it is necessary to neglect some additional higher-order terms. We obtain the following WKB approximations for ϕ and η

$$\phi_n(x^*) \sim \alpha_n (H^*)^{1/4} \sin\left[\lambda_n \Psi(x^*) + \theta_n\right] \tag{2.16a}$$

$$\eta_n(x^*) \sim \frac{A_n}{(H^*)^{1/4}} \cos\left[\lambda_n \Psi(x^*) + \theta_n\right] \tag{2.16b}$$

where $\Psi(x^*) = \int_0^{x^*} [H^*(s)]^{-1/2} ds$, and $\alpha_n = -A_n \sqrt{g H_0}$.

To apply the multi-armed model, Equations (2.16a) and (2.16b) are substituted into Equation (2.10) to give

$$\sum_{i=1}^{N} \sqrt{g H_i(1)} \tan\left(\omega_n \tau_i \int_0^1 \frac{ds}{\sqrt{H_i^*(s)}} + \theta_n\right) = 0 \tag{2.17}$$

where the value of θ_n is found by applying **BC1** Equation (2.16a). If $H^*(0) \neq 0$, then $\theta_n = 0$; however, if $H^*(0) = 0$ then $x^* = 0$ is a singular point and additional work is necessary to determine θ_n and ensure consistency.

Endpoint singularities

For $H^*(0) = 0$, the point $x^* = 0$ is a singular point. If this singularity is integrable, then a modified turning point analysis can be used for ϕ (see Hinch, 1991, p. 133-134). An "inner solution", ϕ_{I}, is developed near the singular point, while an "outer solution", ϕ_{II} (given by Equation (2.16a)), exists through the rest of the domain. Then these solutions are matched by setting

$$\lim_{x^* \to \infty} \phi_{\mathrm{I}}(x^*) = \lim_{x^* \to 0} \phi_{\mathrm{II}}(x^*).$$

To find the inner solution, $H^*(x^*)$ is expanded in a Taylor series about $x^* = 0$. The first non-zero term

$$H^*(x^*) \sim x^* \left[\frac{dH^*}{dx^*}\right]_{x^*=0} \text{ as } x^* \to 0 \tag{2.18}$$

is substituted into Equation (2.2b), and ϕ_{I} is the solution to the resulting ODE. Here, this gives $\phi_{\mathrm{I}}(x^*)$ in terms of the zero-order Bessel function, $\mathrm{J}_0(z)$. The behaviour $\lim_{x^*\to\infty} \phi_{\mathrm{I}}(x^*)$ is given by the 'large argument' expansion of $\mathrm{J}_0(z)$.

The $x^* \to 0$ behaviour of $\phi_{\mathrm{II}}(x^*)$ is given by substituting Equation (2.18) into Equation (2.16a) and calculating the corresponding function Ψ. Matching these solutions results in $\theta_n = -\pi/4$ for all n. Because Equation (2.16b) can be derived from Equation (2.16a), this value of θ_n can be used in both equations, and so the multi-armed model can be used with the WKB approximation accounting for endpoint singularities by using Equation (2.17) with $\theta_n = -\pi/4$. However, with this approximation, $\eta(x^*)$ is still singular at $x^* = 0$. While this doesn't necessarily invalidate the use of Equation (2.17), it would be desirable to have η bounded as $x^* \to 0$. To account for this behaviour it is necessary to construct a higher order approximation for $\eta(x^*)$.

If $\eta = Y(x^*)(H^*)^{-1/2}$, then Equation (2.2a) becomes

$$\frac{d^2Y}{dx^{*2}} + \left(\frac{\lambda^2}{H^*} + \frac{1}{4H^{*2}}\right) Y = 0.$$

In Equation (2.16b), the final term $Y(4H^{*2})^{-1}$ was neglected as $\lambda \to \infty^+$, but if $H^*(0) = 0$, then the two coefficients of Y can be of comparable order near $x^* = 0$ and so that term should not be neglected. Retaining this term gives

$$\eta_{\mathrm{II}} \sim \frac{A_n}{\left(\lambda^2 H^* + \frac{1}{4}\right)^{1/4}} \cos\left(\int_0^{x^*} \sqrt{\frac{\lambda^2}{H^*(s)} + \frac{1}{4H^*(s)^2}}\, ds + \psi_n\right) \tag{2.19}$$

in the outer region. To determine ψ_n, a similar matching procedure as above can be employed. However, the integral inside of the cosine in Equation (2.19) will not converge if $H^* \propto x^*$ as $x^* \to 0$, so the expansion Equation (2.18) cannot be used. Instead, assume

$$H^*(x^*) \sim H^*_{1/2}\sqrt{x^*} \text{as } x^* \to 0$$

where $H^*_{1/2}$ is some constant. Making this substitution in Equation (2.2a) allows for solutions in terms of Bessel functions of order 1/3. Then matching gives $\psi_n = -5\pi/12$ as $\lambda \to \infty$. However, for small λ (which is the scenario of interest) the inner and outer solutions do not match.

2.3 Discussion

2.3.1 The use of Merian's formula in multi-armed lakes

It is the intuition of some researchers that a first approximation of modal periods in a multi-armed lake can be made by applying Merian's formula along the longest longitudinal extent of the lake and ignoring other arms (e.g. Caloi and Spadea, 1958; Imam et al., 2013b; Laval et al., 2008; Malinina and Solntseva, 1972). While Rudnev et al. (1995) suggests that this approach may be inaccurate for higher modes, the present model indicates that in some cases this formula may approximate the correct results for the first mode. Given the TE conditions on τ, the first mode will exhibit a decoupled response in which only two of the arms of the lake are active in the response; in this case it is clear that Merian's formula applied along those active arms should produce modal periods that agree with this simplified model.

Surprisingly, a case can also be made for the "first-guess" accuracy of Merian's formula in the TNE or TM cases. To explain the success of this approach, consider the behaviour described in Section 2.2.3: frequencies ω_n will be located between successive asymptotes of Equation (2.10) when considered over a range of ω. For example, for the flat bottomed case, asymptotes will be located at all $(2n-1)\pi(2\tau_i)^{-1}$, $n \in \mathbb{Z}^+$, so the the location of the first mode will be constrained to

$$\frac{\pi}{2\tau_1} < \omega_1 < \frac{\pi}{2\tau_2} \tag{2.20}$$

where $\tau_{1,2}$ are the two largest values of τ_i. Consider the case $H_{0,1} = H_{0,2} = H_0$, then $\tau_1 > \tau_2$ implies $L_1 > L_2$. The frequency predicted by Merian's formula applied along total length $L = L_1 + L_2$ (the longest extent of the lake) is $\omega = \pi\sqrt{gH_0}(L_1 + L_2)^{-1}$. Substituting these values into Equation (2.20) produces

$$\frac{\pi\sqrt{gH_0}}{2L_1} < \frac{\pi\sqrt{gH_0}}{L_1 + L_2} < \frac{\pi\sqrt{gH_0}}{2L_2},$$

or equivalently

$$2L_1 > L_1 + L_2 > 2L_2.$$

We see that for $L_1 > L_2$ this is consistent, and so the frequency predicted by Merian's formula provides a good approximation of the fundamental frequency predicted given by Equation (2.14).

2.3.2 The impact of cross-sectional variation

Depth variation

The classic approach to estimating modal periods using Merian's formula suggests that modal periods, T_n, follow a harmonic progression given by

$$T_n = T_1 \left(1, \frac{1}{2}, \frac{1}{3}, \frac{1}{4}, \dots\right) = \frac{T_1}{n}.$$

Chrystal (1905) showed that in simple lakes, these ratios of modal periods do not follow this harmonic sequence when depth variation is accounted for. However, his work did not explicitly discuss the impact of depth variation on the fundamental mode. By considering an approach similar to that employed in Section 2.3.1, it is possible to investigate the impact of depth variation in multi-armed lakes.

As described in Sections 2.2.3 and 2.3.1 The frequency of the fundamental mode is constrained between the first two asymptotes: $\Omega_1 \leq \omega_1 \leq \Omega_2$. By comparing the constant bottom (subscript C) model and the linearly varying (subscript ℓ) models, it is evident that the locations of these asymptotes ($\Omega_{1,2} = z_1^\eta \tau_{1,2}^{-1}$ where $\tau_{1,2}$ are the two largest values of τ_i) are relatively insensitive to changes in depth variation. If

$$H_i = \frac{H_\ell}{L_i} x$$

then

$$\begin{aligned}(H_{0,i})_\ell &= H_\ell \\ (H_{0,i})_C &= \frac{1}{L_i} \int_0^L \frac{H_\ell}{L_i} x dx = \frac{1}{2} H_\ell\end{aligned}$$

and

$$\begin{aligned}(\tau_i)_\ell &= \frac{L_i}{\sqrt{g H_\ell}} \\ (\tau_i)_C &= \frac{L_i}{\sqrt{g\left(\frac{1}{2} H_\ell\right)}} = \sqrt{2}(\tau_i)_\ell\end{aligned}$$

As in Section 2.3.1, for the constant bottom $(z_1^\eta)_C = \pi/2$; for the linearly

varying bottom $(z_1^\eta)_\ell$ is the first zero of $\mathrm{J}_0(2z)$, so $(z_1^\eta)_\ell \approx 1.202$. So

$$(\Omega_{1,2})_\ell \approx \frac{1.202}{(\tau_{1,2})_\ell}$$
$$(\Omega_{1,2})_C = \frac{\pi}{2\sqrt{2}(\tau_{1,2})_\ell} \approx \frac{1.111}{(\tau_{1,2})_\ell}.$$

Thus, $(\Omega_{1,2})_C \approx (\Omega_{1,2})_\ell$. Because the first modal frequency ω_1 will be constrained by these asymptotes, we see that the prediction of the fundamental mode is not overly sensitive to depth variation.

In contrast, as predicted in simple lakes by Chrystal (1905), higher modes are expected to be much more sensitive to depth variation. The harmonic sequence of modal periods predicted by Merian's formula is a result of the even spacing between successive zeros z_m^ϕ when a constant bottom bathymetry is used. For lakes of varying depth, these zeros will not be uniformly spaced and so the periods of higher modes deviate from the harmonic sequence. In multi-armed lakes modal periods are predicted based on an interaction of the zeros z_m^η and so the impacts of depth variation will compound.

The spatial structure of the mode-shapes of higher modes will also be impacted by depth variation. Specifically, for forms of H^* that shoal towards the ends of the lake ($H^*(0) \to 0$ and $\frac{dH^*}{dx^*} > 0$), such as the linearly-varying depth case, the amplitude of the mode-shape function η decreases with increasing distance from the origin. This is visible in the analytically defined solution to the linearly varying depth case ($\eta(x) \propto \mathrm{J}_0(\lambda\sqrt{x^*})$), but also in the case of arbitrary depth variation Equation (2.16b) ($\eta(x) \propto [H^*]^{-1/4}$). As a result, the highest predicted peak in η occurs at $x_i^* = 0$ (i.e. at the ends of the arms), and as the mode number increases more of the domain is governed by lower amplitude waves. This will lead to a behaviour where deflections are increasingly localized to only the very tips of the domain.

The WKB approximation that was put forward as a way of estimating the response in lakes of arbitrary depth variation allows for some further insight into the impact of depth variation on the response of the lake. The model presented here indicates that relative values of the parameter $\tau_i = L_i(gH_{0,i})^{-1/2}$, called the "wave travel time" predicts which of the the two classes of behaviour will be exhibited: either a whole-lake response or a decoupled response. When considering an arbitrary bottom profile along each arm, the WKB approximation (Equation (2.17)) suggests that the condition $\tau_i = \text{constant}$ is replaced by

$$\int_0^{L_i} \frac{ds}{\sqrt{gH_i(s)}} = \text{constant}. \tag{2.21}$$

In fact, this change in condition confirms the intuition that the time of travel of a progressive wave in a given arm has an influence on whether or not a decoupled response should be expected. In a channel of varying depth, the barotropic wave speed is $c(x) = \sqrt{gH(x)}$. If a wave in such a channel travels a distance dx with a speed $c(x)$, then the time of travel is $dt = dx[c(x)]^{-1}$, and the total travel time over the domain x is $t = \int dt = \int dx[c(x)]^{-1}$, which is the quantity described by Equation (2.21). This indicates that Equation (2.21) generalizes the condition $\tau_i = \text{constant}$ to an arbitrary depth profile.

Unfortunately, the WKB method faces limitations in it's ability to correctly predict the modal periods of multi-armed lakes. In simple systems the WKB approximation can provide very good estimates of the eigenvalues of an ODE, particularly for higher modes (Bender and Orszag, 1999). For multi-armed lakes, both η and ϕ need to be estimated. While Equation (2.2b) is in a form compatible with the WKB approximation, in order to approximate the solution to Equation (2.2a) additional steps must be taken. η has to be determined either from ϕ through Equation (2.3), or through a variable substitution to convert Equation (2.2a) into a WKB form. In both of those cases, the $\lambda \to \infty^+$ condition is used to neglect higher-order terms in order to produce a tractable result. In the variable substitution method, additional terms can be retained to preserve accuracy (Equation (2.19)), but if $H^*(0) = 0$ (i.e. if there are endpoint singularities), then an additional approximation must still be made in the η equation in order to match the inner and outer solutions near the singular point. Because of the additional approximations necessary for the η function, the level of accuracy of the equations for ϕ and η will not match. Modal periods are predicted based on a ratio of these functions (Equation (2.10)) so this accuracy mismatch indicates that the condition **CC2** is unable to guarantee total mass conservation across the lake; this effect will be most pronounced for lower modes. The functions ϕ and η may provide independently good approximations for the mode-shapes if the correct frequencies ω_n are supplied, but it is unlikely that the WKB method will accurately predict those frequencies for the lowest modes.

Width variation

As developed, the model assumes a constant width along arms of the lake $b(x) = b$, so cross-sectional variability occurs solely due to variations in lake depth. In many fjord-type lakes, this is a reasonable approximation for barotropic modes as arm width may vary much more gradually than total

depth. However, it is trivial to re-write Equation (2.2a) (and similarly Equation (2.2b)) in terms of the total cross-sectional variation $S(x)$ (Proudman, 1953):

$$\frac{d}{dx}\left(S(x)\frac{d\eta}{dx}\right) + \lambda^2 b(x)\eta = 0. \tag{2.22}$$

Accounting for total cross-sectional variation in the model developed in the present study would likely increase accuracy of the results, and could be done with minimal adaptation. However, it is expected that the behaviour and important parameters predicted by such a modified model would not change from the present results. And while adapting the mathematically description may be relatively simple, defining physical parameters such as cross-sectional area in the vicinity of the confluence may be difficult in actual lake systems.

2.3.3 Extensions of this model

More complex geometries

Of interest is the application of the techniques described here to more complex geometries. For example, more complex branching multi-armed lakes can also be thought of as a series of one-dimensional reaches that are coupled by using boundary conditions at a variety of connection points. Unfortunately, the solutions for these more systems can quickly become cumbersome. For an "H"-shaped geometry (Figure 2.2), the equation analogous to Equation (2.14) is

$$\begin{aligned}\frac{1}{\sqrt{gH_{0,11}}\tan(\omega_n\tau_{11}) + \sqrt{gH_{0,12}}\tan(\omega_n\tau_{12})} \\ + \frac{1}{\sqrt{gH_{0,21}}\tan(\omega_n\tau_{21}) + \sqrt{gH_{0,22}}\tan(\omega_n\tau_{22})} \\ + \sqrt{gH_{0,M}}\tan(2\omega_n\tau_M) = 0\end{aligned} \tag{2.23}$$

Predictably, in this case it is not straightforward to understand possible decoupled responses (which might occur if there are nodal lines at either of the two confluences). So while these ideas may have merit, it would likely be easier to predict the response of branched multi-armed basins using numerical methods.

In complex geometries other than multi-armed lakes, some analogous procedure as discussed here may be appropriate. If Equations (2.2a,b) (or their two-dimensional equivalents) can be simplified by considering only the

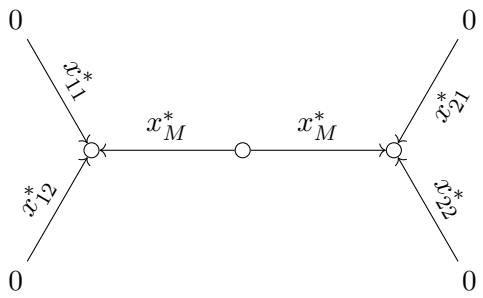

Figure 2.2: Schematic representation of an "H"-shaped multi-armed geometry

overriding geometric feature then insight may be gained into the impact of that feature on the response. In the present study, no other geometries are considered.

Baroclinic Modes

Longuet-Higgins (1952) (among others) have shown that for a perfectly two-layer system, the barotropic and baroclinic modes can be effectively separated. The barotropic modes will respond as per the modes of an equivalent homogeneous body of water. The baroclinic modes will be governed by a set of equations of the same form as the barotropic modes, but with a modified wave speed given by $c^{(2)} = (g' H_{\text{eff}})^{1/2}$. Here, the "reduced" gravity, g', is dependent on the relative densities of the upper and lower layers, $\rho_{1,2}$ respectively:

$$g' = g\left(\frac{\rho_2 - \rho_1}{\rho_2}\right).$$

The "effective depth", H_{eff}, is given by the harmonic mean of the upper and lower layer thicknesses $H_{1,2}$ (which add to the total depth $H_1 + H_2 = H(x)$):

$$H_{\text{eff}}(x) = \frac{H_1 H_2}{H_1 + H_2} = H_1\left[1 - \frac{H_1}{H(x)}\right].$$

For baroclinic seiching, if the non-dimensional depth H^* and eigenvalues λ_n are defined as $H^* = H_{\text{eff}}(x)(H_0)^{-1}$ and $\lambda_n = \omega_n L(g' H_{\text{eff}})^{-1/2}$, then Equations (2.2a) and (2.2b) can be used to describe the mode shapes of interface deflection $\eta = \eta^{(2)}$ and bottom-layer flow $\phi = \phi^{(2)}$, and so the model described in this study can be applied to predict the frequencies and mode-shapes of baroclinic modes.

Fjord-type lakes are typically very deep with steep side-walls, so the total depth $H(x) \gg H_1$ through most of the lake, and therefore $H_{\text{eff}} \sim H_1$.

This is important because, while barotropic seiching is sensitive to the depth variation $H(x)$, the effective depth H_{eff} used in the formulation of the baroclinic wave equations is essentially constant except near the shore. A choice for the characteristic depth H_0 to be equal to the upper layer thickness, $H_0 = H_1$, results in $H^* \sim 1$. This suggests that using a constant bottom depth variation in the simplified analytical model should be appropriate for most cases of baroclinic seiching, regardless of the actual form of $H(x)$. Adapting Equation (2.14) to the parameters that describe baroclinic modes gives

$$\sum_{i=1}^{N} \tan\left(\frac{\omega_n L_i}{\sqrt{g' H_{\text{eff}}}}\right) = 0 \tag{2.24}$$

The lack of variation in H_{eff} has an additional effect on the application of this model. Because $H_0 = H_{\text{eff}} \sim H_1$, and H_1 is typically spatially constant, $H_{0,i} = \text{constant}$. So the TE condition of $\tau_i = \text{constant}$ simplifies to $L_i = \text{constant}$ for the decoupling of baroclinic waves.

In contrast to barotropic modes, whose higher horizontal modes are difficult to predict due to sensitivity to depth variation, it is expected that Equation (2.24) will accurately represent higher baroclinic modes. Of course, those modes are still modified by variation of the cross-sectional area along the thalweg (Mortimer, 1979), so a truly accurate representation of those higher modes would have to modify the model to consider width variation.

2.3.4 Similarity to Neumann's impedance method

As discussed in Section 1.2.2, the impedance theory developed by Neumann (1944, as cited in Defant, 1960) provides an analytical methodology for calculating modal frequencies of connected basins in lakes and bays. Defant (1960) includes an example of this method using a three-armed geometry analogous to that investigated here (see Figure 76 of his text). For the closed system, this results in the following equation for predicting the modal frequencies:

$$b_1 c_1 \tan\left(\frac{\omega L_1}{c_1}\right) + b_2 c_2 \tan\left(\frac{\omega L_2}{c_2}\right) + b_3 c_3 \tan\left(\frac{\omega L_3}{c_3}\right) = 0,$$

where c_i is the wave speed in arm i, $c_i = (g H_i)^{1/2}$, and b_i is the width of arm i. If $b_1 = b_2 = b_3$, this is identical to Equation (2.14). This technique similarly reproduces Equation (2.23) for the geometry described by Figure 2.2. However, the impedance method does not properly account for the possibility of nodal lines positioned at the location of the confluence. Because of this

limitation, the impedance method is unable to reproduce the decoupled modes predicted by the present model, which is one of the central results.

Due to the simplicity of the impedance method, for multi-armed or interconnected basins of any geometry in which a decoupled response is not suspected to occur this method will likely yield a reasonable approximation of the longest mode periods without the need of a numerical approach. The sensitivity of higher modes to depth variation (which is not included in this method) would still preclude accurate predictions of those modes. However, through this model, both depth and width variation can be accounted for by splitting a single basin into a number of sub-basins each with it's own depth and width (i.e. assuming a "stepped" bottom bathymetry); such a procedure does increase the complexity of the resulting equation for determining ω_n.

2.4 Conclusions

This chapter develops a simplified analytical model to identify the key geometric parameters responsible for the sieche response of fjord-type multi-armed lakes. In simple elongated lakes, the period of the fundamental mode is given by Merian's formula, in which the length of the basin and the shallow-water wave speed are both key parameters. As expected, these parameters are similarly important in multi-armed lakes; however, they are taken individually for each arm of the lake. The model suggests two different classes of behaviour based on the relative values of a parameter τ, defined as $\tau_i = L_i(gH_{0,i})^{-1/2}$, which represents the time of travel of a progressive shallow-water wave moving longitudinally in the i^{th} arm of the lake. These behaviours differ based on the case of $\tau_i = \text{constant}$ (denoted the TE case) or $\tau_i \neq \text{constant}$ (denoted the TNE case).

The TNE may be expected to be more common in real water bodies. In this scenario, all of the arms of the lake are active in every mode; the behaviour observed by Buzzi et al. (1997) and Guyennon et al. (2014) in Lake Como in which the eastern arm does not act for some modes, is not present for the TNE case. Due to this structure, this case is referred to as a "whole-lake mode". In this case, the modal frequencies ω_n are given by the solution to a transcendental formula, Equation (2.10), whose specific form is based on the form of depth variation of the arms. In contrast, two equations exist for the modal frequencies for the TE case, both of which are simple and analytic provided that the zeros $z_n^{\eta,\phi}$ are known. The set of modal frequencies given by these two formula correspond to either a node or an anti-node appearing at the confluence point. The modes that have

Table 2.1: Summary of modal frequency equations for the TE and TNE cases, as developed in Section 2.2.2. In the TE model, the $\xi_n = 0$ case corresponds to nodes located at the confluence point, while $\xi_n = 0$ corresponds to anti-nodes being located at the confluence point. In the TNE model, ξ_n must be non-zero.

	TE	TNE
$\xi_n = 0$	$\omega_n = \frac{z_n^\eta}{\tau}$	-
$\xi_n \neq 0$	$\omega_n = \frac{z_n^\phi}{\tau}$	$\sum_{i=1}^{N} C_i \frac{\phi(1, \omega_n \tau_i)}{\eta(1, \omega_n \tau_i)} = 0$

a node occurring at the confluence exhibit a decoupled behaviour in which only 2 of the arms of the lake are active, while the remainder of the lake is quiescent. These "decoupled modes" have an eigenvalue multiplicity given by the binomial combination ${}_NC_2$, where N is the total number of arms of the lake. If a subset of the arms have equal wave travel times, a "mixed-case" (TM) can occur, which is an amalgamation of the two results. The whole-lake modes will be calculated as normal using Equation (2.10) while additional decoupled modes are calculated using Equation (2.12a) and exist for only the arms with repeated τ_i. The equations for determining the modal frequencies for the TE and TNE cases are summarized in Table 2.1.

The whole-lake versus decoupled behaviour is developed for the general form of the underlying equations, and so is independent of the actual form of the depth variation of the lake. While general solutions do not exist for an arbitrary bottom profile, the WKB asymptotic method is used to approximate solutions in this case. While limitations of the WKB method may prevent accurate prediction of lower modes, this method reiterates that the ratios of the wave travel time along the longitudinal extents of each of the arms is the parameter of interest in predicting a decoupled or whole-lake response.

Interestingly, despite the complexities associated with having multiple arms, this model suggests that the first fundamental period can still be estimated with reasonable accuracy by assuming a constant depth in each arm and applying Merian's formula along the two arms that create the longest extent. More strictly, the formula should be applied across the arms that have the two highest values of τ_i. This behaviour is retained for both the TE and TNE cases of τ_i. Contrary to the fundamental mode, which appears to be relatively independent of depth variation, the periods of higher modes are very sensitive to the form of $H(x)$.

While developed for barotropic motions, the separation of vertical modes suggests that this model is equally valid for baroclinic seiching. In fact, in an idealized two-layered system, the limited spatial variability in H_{eff} suggests that it suffices to take only the constant-bottomed variation of this model. Then the changes in wave travel time between arms of the lake is determined by the length of arm, so the condition that determines whether a decoupled response is expected is simply if $L_i = \text{constant}$. While additional complexity may exist for baroclinic modes (such as the influence of the Coriolis force, or the increased likelihood of non-linear effects), the present model should still improve on the current ability to make quick, rough estimates of modal periods and shapes

The present model predicts behaviours only for a specific type of surface geometry. Nonetheless, it exemplifies the level of additional insight that can be gained through the application of a simplified approach. Before now, there was no consensus on whether a decoupled response was a general feature of multi-armed geometries. Now, not only is this decoupling explained, but a criteria exists to predict if it may happen in a given lake. By reducing the two-dimensional domain of the lake into a set of coupled one-dimensional domains, the model considers only the defining geometric feature of multi-armed lakes. A similar approach may be taken to consider the influence of other geometric features in different lake classifications.

Chapter 3

Barotropic seiche modes in two fjord-type Y-shaped lakes

3.1 Introduction

In lakes with low hydraulic throughflow, water quality is modulated by physical processes that induce currents and mixing in the lake. Given the importance of seiching in driving currents that lead to the transport of mass and materials through the lake, these events are of particular importance in lake systems. For complex or multi-armed lakes, prediction of seiche mode-shapes and periods typically relies on case-by-case application of numerical models or detailed field studies, and so generalizations are difficult to make. The simplified analytical model developed in Chapter 2 provides a framework for understanding the role of geometry in fjord-type multi-armed lakes which can be used to provide context for observed or numerically modelled results.

One behaviour Chapter 2 predicts is that the first mode of a multi-armed lake should conform to simple linear oscillation of the longest extent of the lake which could be roughly estimated by applying Merian's formula along that extent. This justifies the assumptions made by Malinina and Solntseva (1972, as cited in Rudnev et al., 1995) in Lake Onega, Laval et al. (2008) in Quesnel Lake, Caloi and Spadea (1958) in Lake Como, and Imam et al. (2013b) in Nechako Reservoir. However, the model indicates that additional arms and complexities cannot be neglected for higher modes.

Perhaps the most interesting result in Chapter 2 is that it is possible for multi-armed lakes to exhibit a response in which one or more arms are decoupled from the main body of the lake and do not oscillate. A combination of field and numerical study of internal (baroclinic) seiching within Lake Como found such a result, where for some modes the eastern arm of the lake is inactive in the response (Guyennon et al., 2014). A numerical scheme used by Buzzi et al. (1997, hereafter BGS) showed that the same holds true

for surface (barotropic) seiche modes in Lake Como. Rudnev et al. (1995) finds that barotropic oscillations in some arms or bays of Lake Onega act in isolation, with near-zero deflection in the remainder of the lake; however, it is difficult to commensurate the geometry of Lake Onega with the system studied in Chapter 2. In contrast, Imam (2012) and Imam et al. (2017) find no such decoupling in multi-armed Nechako Reservoir, nor do Carter and Lane (1996) find any decoupling in multi-armed Lake Te Anau. For radial multi-armed lakes (where all of the arms meet at a single confluence point) such as "Y"-shaped lakes, the model in Chapter 2 provides a geometric criteria to predict whether a decoupled behaviour is possible; however, the model is developed only for an idealized case. It will be instructive to consider the application of the simplified model to real lake geometries.

This chapter investigates two "Y"-shaped lakes: Lake Como, located in Northern Italy; and Quesnel Lake, located in Western Canada. While the lakes are different sizes, they have a number of similarities. Both lakes are fjord-type lakes with a three-armed geometry. As is typical of fjord-type lakes, the arms of both of these lakes are narrow and elongated with steep side walls. In the context of the model developed in Chapter 2, these two lakes exemplify two different classes of behaviour. As identified by BGS and Guyennon et al. (2014), Lake Como appears to exhibit decoupling of the eastern arm. Similar studies have not been conducted in Quesnel Lake and so it is not yet known if a decoupled behaviour exists; however, based on the significant differences in length and depth of the arms, the simplified model predicts only whole-lake modes. The two classifications allow for verification of the parameters and behaviours predicted in Chapter 2. The results will be validated using a combination of field observations, and a Finite Element Method (FEM) numerical scheme (see Section 1.2.3). A comparison of the predicted response of both lakes will provide further ability to make general statements about standing wave modes in multi-armed lakes.

3.2 Methods

3.2.1 Site descriptions

Quesnel Lake

Quesnel Lake (Figure 3.1a) is a fjord-type lake, and consistent with that morphotype, it is narrow-armed and deep, with a mean depth of 157 m and a maximum depth of 511 m (Laval et al., 2008). It has an east-west span of 81 km and a north-south span of 36 km. The lake is roughly "Y"-shaped,

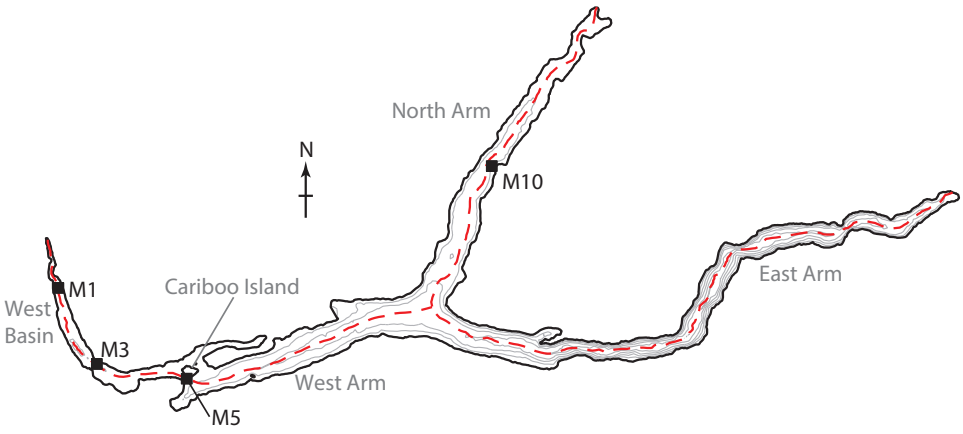

(a) Quesnel Lake

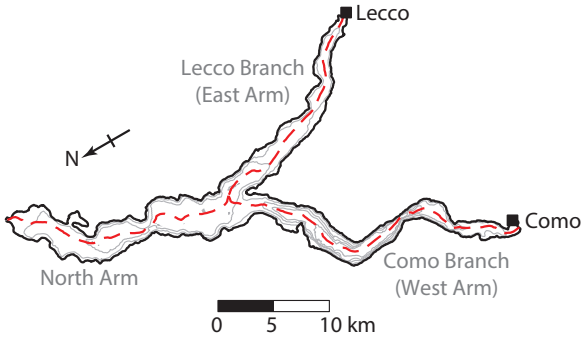

(b) Lake Como

Figure 3.1: (a) Map of Quesnel Lake showing the locations of the moorings (■); (b) Map of Lake Como showing the locations of the communities of Lecco (where the limnograph discussed in Section 3.2.2 was deployed) and Como. In both maps, contour lines are shown every 100 m, and red dashed lines indicate the local thalweg for each arm used in the model discussed in Section 3.3.3. The distance bar in (b) applies to both figures, which are presented to the same scale.

with three arms (the North, East, and West Arms) extending outward from a central junction. At the end of the West Arm, Cariboo Island creates a constriction and shallow sill that separates a distinct sub-basin, the West Basin. This sill is an important feature for understanding baroclinic seiching, and the exchange of deep water between the basins Laval et al. (2008).

Quesnel Lake follows a seasonal stratification pattern consistent with dimictic lakes, modified slightly by pressure effects on the temperature of maximum density due to the great depth of the lake Laval et al. (2012). During summer, the lake is strongly stratified with a warm eplimnion overlying a cold ($\sim 4°C$) hypolimnion; in the winter it experiences weak reverse stratification with cold ($< 4°C$) water overlying warmer ($\sim 4°C$) water. Despite some subtle details caused by the pressure effects, the lake experiences regular seasonal turnovers of the entire water column occurring roughly in December ("fall" turnover), and May (spring turnover) (Laval et al., 2012).

Lake Como

Lake Como (Figure 3.1b) is located in the Lombary Region of Northern Italy, and extends into the southern edge of the Alps. It is smaller than Quesnel Lake, with an east-west span of 26 km and a north-south span of 40 km. Like Quesnel Lake, Lake Como is also "Y"-shaped and fjord-like. One of its three arms extends north from the confluence point, while the other two bifurcate into south-east and south-west pointing arms. The city of Lecco is located near the tip of the western of these two arms while the city of Como is located near the tip of the eastern arm, so these are occasionally referred to as the "Lecco Branch" and the "Como Branch". Despite its smaller size compared to Quesnel Lake, Lake Como is also very deep with a maximum depth of 425 m and a mean depth of 151 m (Guyennon et al., 2014).

In contrast to Quesnel Lake, Lake Como does not experience full seasonal turnover; instead it is considered oligiomictic and fully turns over only occasionally (Guyennon et al., 2014; Morillo et al., 2009; Salmaso and Mosello, 2010). Typical winter turnover only extends to ∼150 m depth (Morillo et al., 2009).

3.2.2 Field study

Surface seiching is characterized by consistent oscillations of the water surface. The natural periods of the oscillatory modes in a lake can be determined through spectral analysis of these water level signals. Peaks in spectral energy will correspond to modal periods.

In evaluating and characterizing the barotropic response of Lake Como, this study builds on the work of BGS, and will draw on the results presented by those authors; no additional field study has been performed. BGS collected water level readings in Lake Como using a limnograph mounted near the community of Lecca (on the south-east arm; see Figure 3.1b). The limnograph recorded water levels on three separate dates: Feb. 17, Feb. 18, and Mar. 1, 1996. The recording intervals were ∼9.5 hours, ∼7.5 hours, and ∼11.7 hours, respectively, and and the limnograph measured water elevation at a rate of 1 sample per minute. With these data BGS were able to identify modal periods using spectral analysis.

To identify surface seiche modes in Quesnel Lake, data are presented from four moorings that were installed in the lake in Nov. 2014 (see Figure 3.1a). Each of the moorings was equipped with an RBR duo T.D. in the upper water column. These instruments recorded total pressure at a sampling period of 4 seconds then these data were averaged over 1-minute. In order to perform frequency analysis, the longest continuous pressure record between mooring servicing was used, which extends from Oct. 2, 2015 to Sept. 15, 2016.

The pressure sensors installed at the moorings measured total pressure; in order to relate total pressure to water level through hydrostatic pressure, the barometric pressure signal must first be subtracted. However, the spectral analysis considers the periodicity of data fluctuations, and so actual water level depth is unimportant. Provided that the barometric pressure fluctuations do not have an oscillatory signature that can be confused with the barotropic response, the identification of seiche modes from total pressure will be relatively insensitive to the barometric pressure. A weather station installed at the Quesnel River Research Centre (QRRC), approximately 1.4 km downstream from the outflow of Quesnel Lake, has intermittent measurements of barometic pressure throughout the period of record of the moorings. These data are available at a 15-minute sampling period so they can be used to rule out the effects of barometric pressure on any oscillatory motion with a period greater than 30 minute (corresponding to the Nyquist frequency).

3.2.3 Modelling

Following convention, we investigate the free-response by considering the homogenous linear shallow-water (LWS) equations. Based on mean depth, the external Rossby radius at Quesnel Lake (latitude 52.5° N) is ∼340 km. The Rossby radius at Lake Como (latitude 46.2° N) is ∼370 km. These

values are both much larger than the scale of each of the lakes, so Coriolis effects are neglected. In the absence of Coriolis forces, the LSW equations are given in a two-dimensional domain as (e.g. Rudnev et al., 1995):

$$\text{Momentum:} \qquad \frac{\partial \boldsymbol{q}}{\partial t} + gH\nabla h = 0 \tag{3.1a}$$

$$\text{Continuity:} \qquad \frac{\partial h}{\partial t} + \nabla \boldsymbol{q} = 0 \tag{3.1b}$$

where $H(x, y)$ is the still water depth, $h(x, y, t)$ is the surface deflection (the total depth is given by $H + h$), $\boldsymbol{q}(x, y, t)$ is the depth-integrated horizontal velocity ($\boldsymbol{q}(x, y, t) = \int_0^H \boldsymbol{u} dz$), and the operator ∇ is defined in along the two horizontal dimensions: $\nabla = (\partial_x, \partial_y)$.

Assuming an oscillatory response, $\boldsymbol{q}(x, y, t) = \boldsymbol{\phi}(x, y)e^{i\omega t}$ and $h(x, y, t) = \eta(x, y)e^{i\omega t}$, Equations (3.1a) and (3.1b) are combined to give the Helmholtz-like equations:

$$\nabla \cdot (H\nabla\eta) + \left(\frac{\omega^2}{g}\right)\eta = 0, \tag{3.2a}$$

$$\nabla^2\boldsymbol{\phi} + \left(\frac{\omega^2}{gH}\right)\boldsymbol{\phi} = 0. \tag{3.2b}$$

Equations (3.2a) and (3.2b) are eigenvalue problems and as such have an infinite number of eigenfunction solutions. These solutions represent the undamped free response modes of the lake surface deflection (η) and horizonal current ($\boldsymbol{\phi}$). The true response of a lake to some external forcing will be composed of these free response modes and, because damping of barotropic seiching is small (Defant, 1960), the observed oscillatory periods should match the predicted periods to a high degree of accuracy.

Two methods are used to determine the solutions to these equations: a numerical solver, and the simplified analytical model developed in Chapter 2. For clarity, this study will present the mode-shapes η_n obtained by solving Equation (3.2a) using these models. While the $\boldsymbol{\phi_n}$ will not be shown, these are obtained from η_n through Equation (3.1a); that is $\boldsymbol{\phi_n} = -i\omega_n gH\nabla\eta_n$ where the imaginary number $i = \sqrt{-1}$ simply indicates that h and $\boldsymbol{q}$ occur 90° out of phase in time. Thus the mode-shape deflections have corresponding horizontal velocities.

Numerical Solver

In a two-dimensional domain, Equation (3.2a) can be solved numerically using the Finite Element Method (FEM; see Section 1.2.3). In FEM, the

modal frequencies and shapes are given by solving for the eigenvalues and eigenvectors of the discretized problem:

$$\mathbf{K}\tilde{\eta} = \Lambda\mathbf{M}.$$

The matrices $\mathbf{K}$ and $\mathbf{M}$ that result from from discretization are large and sparse, so the matrix $\mathbf{M}^{-1}\mathbf{K}$ is large and dense. While the exact eigenvalues and eigenvectors can be computed for such matrices, the size of these matrices may lead to computer memory constraints that limit the ability to solve for them exactly. In this case, approximation methods such as the Lanczos method are employed to estimate eigenvalues (Schwab, 1980). The accuracy of this approximation is determined by the number of iterations (and therefore also has a computational cost).

The numerical scheme employed by BGS used a regular rectangular grid, and considered grid spacings of both 250 m and 500 m. The domain was defined by 2399 active elements in the case of the 250 m grid spacing, and 596 active elements in the case of 500 m grid spacing. The study also considered different values for the "truncation number", *NF*, used in the Lanczos procedure. The results show that the modal periods are sensitive to both grid size and *NF* (see Table 10 in their paper), with the fundamental mode seeing a 2.8 minute change from the lowest predicted result (38.9 min) to the highest (41.7 min). Given the increase in computational power now available since BGS studied barotropic seiching on Lake Como, we repeat the numerical experiments in an attempt to increase the accuracy of the results and reach numerical stability.

As described in Section 1.2.3, the method employed in the present study uses an unstructured grid made up of triangular elements. These elements range in size, with small side-lengths and close spacing where the surface geometry changes more rapidly, and larger side-lengths farther from the boundaries. The FEM method is used for predicting the barotropic periods of both Lake Como and Quesnel Lake. In each lake, the FEM was run on two different mesh densities ("low-density" denoted LDM, and "high-density" denoted HDM) to demonstrate stability of the results. Details of these meshes can be found in Table 3.1. Eigenvalues of the resulting mass and stiffness matrices are determined using the inbuilt Matlab function `eigs`, which approximates eigenvalues using Arnoldi iteration (a generalization of the Lanczos method).

Table 3.1: Details of the two different mesh geometries (LDM and HDM) used in the FEM analysis for Lake Como and Quesnel Lake.

	Lake Como	Quesnel Lake
Low-Density Mesh (LDM)		
nodes	16051	26143
triangular elements	28580	45744
min. side-length	5.26 m	1.0 m
max. side-length	451.3 m	665.1 m
median side-length	76.4 m	75.6 m
High-Density Mesh (HDM)		
nodes	31796	43205
triangular elements	56655	78150
min. side-length	3.61 m	0.64 m
max. side-length	394.2 m	530.4 m
median side-length	50.3 m	58.9 m

Simplified Analytical Model

In addition to the numerical model, we employ the simplified numerical model (SAM) developed in Chapter 2. The basis of this model is that each of the arms of the lakes is considered to be a one-dimensional domain, with seiche motions occurring only along the longitudinal extent of that arm. This conversion transforms the the two-dimensonal vector $\boldsymbol{\phi}(x, y)$ into a one-dimensional scalar quantity $\phi_i(x_i)$ in each arm, with direction given by the geometry of the arm; similarly $\eta(x, y) \to \eta_i(x_i)$ $(i = 1, 2, 3)$. Thus, the PDEs in Equations (3.2a) and (3.2b) are converted into a set of ODEs coupled at the junction of the three arms. This coupling is achieved by imposing the following boundary conditions:

1. continuity of surface height: $\eta_1(L_1) = \eta_2(L_2) = \eta_3(L_3)$; and
2. conservation of mass: $\sum_{i=1}^{3} \phi_i(L_i) = 0$.

SAM's ability to accurately predict the solutions to Equations (3.2a) and (3.2b) is limited by the simplification of the two-dimensional domain as coupled one-dimensional domains, and by the methods by which depth variation is accounted for (discussed further in Chapter 2 and below). This

model is not expected to predict the solutions with the same level of accuracy as the numerical solver (Section 1.2.3), but will instead provide additional context for those results.

The model predicts two different classes of behaviour dependent on the relative values of a parameter, τ_i, within each arm of the lake. This parameter is defined as $\tau_i = L_i(gH_{0,i})^{-1/2}$, where L_i is the along-thalweg length of each arm i and $H_{0,i}$ is some characteristic depth for that arm; physically, τ_i represents the time of travel of a progressive shallow-water wave in the i^{th} arm of a lake. The model predicts two different set of formulae for determining both the modal frequencies (ω_n) and their spatial structure (η_i, ϕ_i) for the two conditions: $\tau_1 = \tau_2 = \ldots = \tau_N$ (denoted TE) and $\tau_1 \neq \tau_2 \neq \ldots \neq \tau_N$ (denoted TNE). In the TE case alternate modes have a multiplicity of eigenvalues and a response in which some arms can be effectively decoupled from the remainder of the lake. In the TNE case all arms are active in each response. A mixed case (denoted TM) is also possible when τ_i is equal only across some of the arms. In this case a subset of the modes can exhibit arm decoupling and need to be predicted using an additional formula.

In the present study we will consider two approximations of depth variation within each arm of each of the lakes: a constant depth in each arm (SAM-CB), and a linearly varying depth in each arm (SAM-LB). In SAM-CB, the characteristic depth for each arm is given by the mean along-thalweg depth of that arm:

$$H_{0,i} = \frac{1}{L_i}\int_0^{L_i} H_i(x_i)dx_i$$

In SAM-LB, the characteristic depth for each arm is given by a least-squares fit of the equation $H_{LB} = (H_{0,i}L_i^{-1})x_i$ to the depth variation $H_i(x_i)$. Based on the values of $H_{0,i}$ determined in each of these methods, the values of τ_i are given in Table 3.2. As shown in the table, for Quesnel Lake, the behaviour is given by the TNE case and so no decoupled response is expected. However, in Lake Como the North Arm and the Lecco Branch ($i = 2, 3$) share the same value of τ_i for both the SAM-CB and SAM-LB models, so we need to consider the TM response.

3.3 Results

3.3.1 Lake Como

The limnographs employed by BGS show oscillations with amplitudes of $\sim 1-2$ cm (see their Figure 5). We report the results of only the limnograph

Table 3.2: Values of τ_i for each i arm for the SAM-CB and SAM-LB models for Lake Como and Quesnel Lake.

		Lake Como		Quesnel Lake	
	i	Arm	τ_i	Arm	τ_i
SAM-CB	1	Como Branch	560 s	West Arm	1203 s
	2	Lecco Branch	505 s	North Arm	965 s
	3	North Arm	505 s	East Arm	900 s
SAM-LB	1	Como Branch	474 s	West Arm	847 s
	2	Lecco Branch	373 s	North Arm	688 s
	3	North Arm	373 s	East Arm	716 s

that measured surface displacement on Feb. 17, 1996, which had both the most energetic and also the most distinct spectral peaks. The periods measured on the other dates are tabulated in their work and show a high level of agreement.

The FEM analysis was applied to Lake Como using both the LDM and HDM meshes (see Table 3.1). The modal periods predicted by the two meshes differed by ≤ 0.1 minutes so these results are views as numerically stable,and we will report only the results of the FEM applied with the HDM. Table 3.3 compares the modal periods predicted using the FEM and SAM to those observed and predicted by BGS.

As seen in Table 3.3, the numerical predictions given by BGS are greater than the modal periods predicted by the FEM analysis performed here, with the most pronounced effect in the fundamental mode. Compared to the observed periods for modes greater than two, the present FEM analysis performs better than BGS's results. It is worth noting that despite the apparent improvement in results given by the present model, the analysis of BGS is still a reasonable measure of the observed periods. The first and second modes can not be spectrally distinguished in the observational data due to the width of the spectral peak centred at $\sim$35 minutes. BGS predict a mode-2 period of 35.3 minutes so they conclude that this peak simply obfuscates the fundamental mode. Considering the results of the present FEM, we believe that the peak cannot be attributed to either one of the first two modes more strongly than the other and represents a combination of the energy of both modes. Re-analysis of the water level time series using different spectral techniques (such as different choices in windowing or pre-whitening) may help improve the separation between these signals,

but given the similarity between the two periods (36.8 min and 32.1 min), it is unlikely that it would be possible to resolve them completely without a much longer time series or higher frequency recording.

Table 3.3: Modal periods, T_n, in minutes for Lake Como. The periods observed by BGS correspond to the measurement period on Feb. 17 and the period modelled by BGS correspond to the 250m grid spacing with NF=2000. SAM-CB and SAM-LB periods marked with an asterisks ($n = 2, 5$) correspond to periods estimated using the TM response so these modes have some decoupled behaviour. The wide spectral peak in observed data makes it impossible to separate the modal periods of the first and second mode; the $n = 2$ value of 35.3 min was attributed by BGS to the second mode, but this may be inaccurate.

	Buzzi et al. (1997)		FEM	SAM	
n	Observed	Modelled	HDM	SAM-CB	SAM-LB
1	-	40.8	36.8	35.6	37.9
2	35.3	35.7	32.1	33.7*	32.5*
3	20.9	22.4	20.3	17.7	22.3
4	15.8	17.0	15.5	11.9	16.4
5	12.8	13.7	12.3	11.2*	14.2*
6	10.2	10.8	9.9	8.8	12.3

Because the limnograph measured water elevation at only one location on the lake, it is not possible to verify the mode-shapes predicted by the models. Instead, the consistency between observed and FEM predicted periods is taken as an indicator of the success of the model. This criterion is typically sufficient for studies of this nature (e.g. Carter and Lane, 1996; Hutter et al., 1982) and so the mode-shapes predicted by the FEM are taken as correct. Figure 3.2 shows the normalized surface deflections in Lake Como corresponding to the first four modes as predicted by both the FEM and SAM (-CB and -LB) analyses.

Notwithstanding the slight difference in predicted modal periods between the present FEM model and the numerical model employed by BGS, there is high fidelity between the mode-shapes of the first two modes predicted with each of these methods (compare Figure 3.2a, $n = 1, 2$ with Figures 3 and 4 from BGS). However, whereas it is clear from the present FEM results that the second mode, T_2, has two nodal lines in its response, BGS only labels one of these as a nodal line in their results. The second nodal line is shown but misrepresented as a surface displacement contour. Interestingly, there is also good agreement between the present mode-shapes and the V1 baroclinic modes presented by Guyennon et al. (2014).

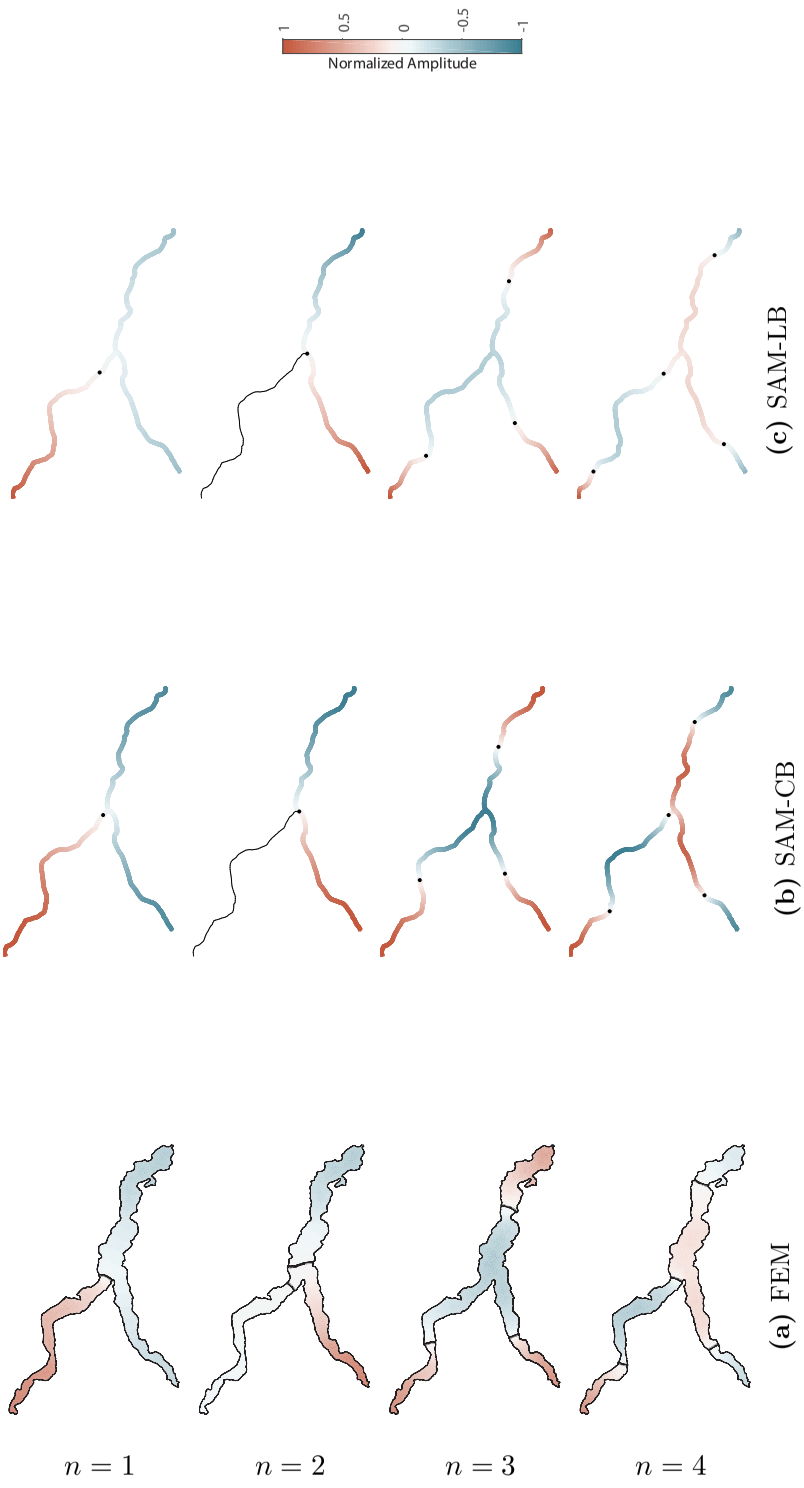

Figure 3.2: Mode-shapes in Lake Como predicted by (a) The FEM model, (b) SAM-CB, and (c) SAM-LB corresponding to the labelled mode numbers, n. Deflections are normalized between -1 (blue) and 1 (red), and nodes are indicated by black contours or dots. The plain black lines in the western arm in (b) and (c) for $n = 2$ represents to the decoupling of that arm for the second mode.

As seen in Table 3.3, in Lake Como both SAM-CB and SAM-LB produce reasonable values of the modal periods when compared to the FEM or observed results. For SAM-CB, these results become increasingly inaccurate for higher modes, whereas SAM-LB is able to retain some level of accuracy in that range. Because higher modes are more sensitive to depth variation, it is not expected that SAM-CB would be accurate for those modes. Despite the error in predicted periods, both SAM-CB and SAM-LB produce qualitatively reasonable mode-shapes (see Figure 3.2). For modes 1, 3, and 4, the correct number of nodal lines, and their approximate locations are well represented.

The mode-2 response in Lake Como corresponds to the decoupled mode predicted by the TM response of SAM. SAM predicts that this mode is a co-oscillation of the North Arm with the Lecco Branch, with a single node at the confluence point and zero deflection in the Como Branch. As seen in the FEM results, this prediction is a reasonable representation of the response. The FEM predicted mode-shape has two nodal lines, both very near each other and in the vicinity of the confluence point. The maximum deflection (normalized to range from -1 to 1) between these nodes is $\sim$+0.05 before entering the eastern arm. The deflection at the tip of the Como Arm is $\sim$-0.06. Due to the very small deflections in this arm, Guyennon et al. (2014) and BGS both describe the second horizontal mode as exhibiting a decoupled response of the Como Branch. The mode-shapes predicted by Guyennon et al. (2014) show that the fifth mode also shows decoupling of the Como Branch. In SAM, an additional decoupled response also occurs for the fifth mode (see Table 3.3).

Despite the success of SAM in predicting the decoupled response in the Como Arm, the actual choice of the location of the confluence point (and thus the values of τ_i) is subjective. An alternate choice of confluence point in Lake Como results in a complete TNE case, where the values of τ_i in each arm are similar but unequal. This indicates that the criterion that determines whether or not decoupling is expected to occur is sensitive to choices made by the individual researchers. Fortunately, the results predicted by SAM were not overly sensitive to this choice. When this analysis was repeated with a different confluence point, the predicted modal periods did not shift by any greater than 1 minute and the mode-shapes were not strongly affected. While the Como Branch no longer experienced a zero-deflection, it did have very small values for deflection (similar to the FEM model). This indicates a robustness of SAM to such subjective choices.

3.3.2 Quesnel Lake

Pressure signals from all stations across Quesnel Lake show consistent high-frequency, low amplitude (less than approximately 0.05 dbar) oscillations for the entire period of record. Larger, transient surface displacements (pressure variations up to approximately 0.15 dbar that last from 12-24 hours) occurred occasionally throughout the record. Both types of oscillatory signals are attributed to surface seiching; however, the transient oscillations are likely triggered by wind storms and are more consistent with the typical schematic representation of seiching. Spectral analysis of these pressure and water level data (Figure 3.3) reveal a number of distinct peaks, which are tabulated in Table 3.4.

Spectral analysis was also performed on the barometric pressure signal (not shown). This analysis showed peaks at the diurnal and semi-diurnal frequencies with a steady decay towards the Nyquist frequency. A small peak at the third harmonic of the diurnal signal ($T = 8$ hr) appears but is not statistically significant. No energetic peaks exist within the frequency range corresponding to barotropic motions in the lake.

As with Lake Como, the difference in the periods predicted by the FEM analysis using either the HDM or LDM grids were ≤ 0.1 minutes and so only the HDM results are presented. The FEM predicted periods correspond to the peaks in spectral response; however, in all cases the solver overestimates the periods compared to the observations (see Table 3.4). This may be due, in part, to a more limited spatial coverage of bathymetric data available for Quesnel Lake compared to Lake Como, particularly in the deeper sections of the lake (such as the East Arm). Despite these differences, the FEM appears successful in its ability to identify the observed periods.

Table 3.4: Modal periods, T_n, in minutes for Quesnel Lake as measured from observational data, and model results.

	Observed	FEM	SAM	
n		HDM	SAM-CB	SAM-LB
1	75.3	79.0	75.1	70.9
2	61.1	62.4	63.2	60.6
3	46.0	47.8	33.3	40.6
4	33.5	35.4	24.8	30.8

There are a number of significant peaks in Figure 3.3 at all mooring stations at higher frequencies (30-minute periods and below). The periods of

these modes are less than the 30-minute period corresponding to the Nyquist frequency of the barometric pressure signal. While there is no reason to expect that the atmospheric pressure would have any oscillatory structure with frequencies in this range, it is not possible to separate hydrostatic pressure from atmospheric pressure for these frequencies. Furthermore, higher modes are much more sensitive to bathymetic variation and so prediction of these modes can be less accurate; note that for the modes presented in Table 3.4 the FEM model has errors of $\sim 2-4$ min, and the difference between periods of these higher modes can be < 1 min. For these reasons, the present discussion will focus only the lowest frequency modes.

The η-eigenmodes predicted by the FEM are shown in Figure 3.4, where they are compared to those predicted using both SAM-CB and SAM-LB.

The spatial coverage of mooring data in Quesnel Lake is insufficient to deduce the spatial structure of the mode-shapes from observational data alone. However, the number of moorings and their distribution does permit some validation of the predicted mode-shapes. Table 3.5 compares the energy associated with the spectral peaks at the different station locations and the associated energy at the same locations from the numerical predictions. These results show a good level of agreement between observed and modelled mode-shapes.

Table 3.5: The energy associated with each n mode, relative to the energy measured at station M1. The observed values are taken from the spectral peaks shown in Figure 3.3. The predicted values are taken from the displacements given by the FEM analysis shown in Figure 3.4; energy is proportional to displacement squared. No observed value is given for M5 for $n = 2$ because there is no evident spectral peak to measure

	Observed				FEM			
n	M1	M3	M5	M10	M1	M3	M5	M10
1	1.00	0.73	0.09	0.02	1.00	0.71	0.06	0.01
2	1.00	0.63	-	3.36	1.00	0.56	0.01	3.07
3	1.00	0.37	0.31	0.01	1.00	0.32	0.36	0.00
4	1.00	0.11	0.86	0.57	1.00	0.02	0.86	0.60

In Quesnel Lake, SAM-CB provides a good estimate of the first two periods of oscillation, but is unable to accurately predict the periods of higher modes (Table 3.4). While SAM-LB does improve on the accuracy of the results for modes 3 and 4, the increase is only marginal and is offset by a decrease in accuracy in modes 1 and 2. Along-thalweg depth variation in Quesnel Lake is poorly described by a linear model, particularly in the East

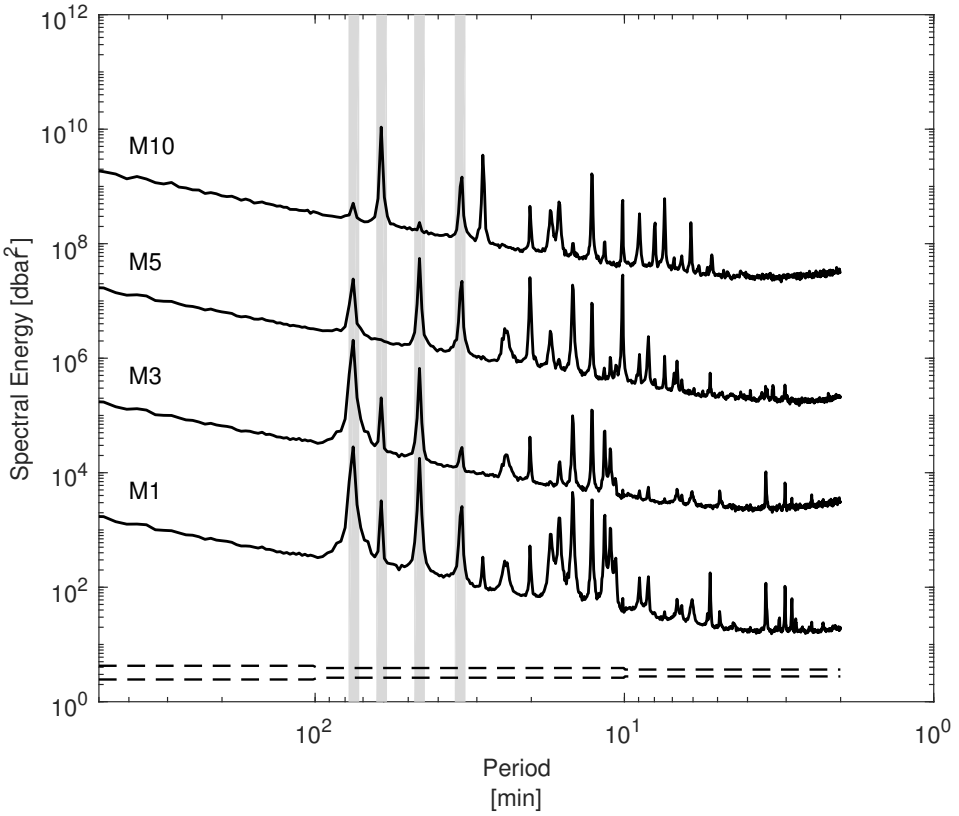

Figure 3.3: Spectral energy computed for pressure recorded at the moorings. For clarity, the lowest signal (M1) is shown with true values, while subsequent signals are each shifted vertically by a factor of 10^3. Significant energy is also contained in periods longer than 500 minutes but no peaks of significance or interest are contained in that range; the choice of axis limits is made to highlight the spectral peaks associated with barotropic modes. Vertical grey bands highlight the peaks tabulated in Table 3.4 and discussed through the text. 95% confidence bounds are shown by dashed lines along the bottom of the panel.

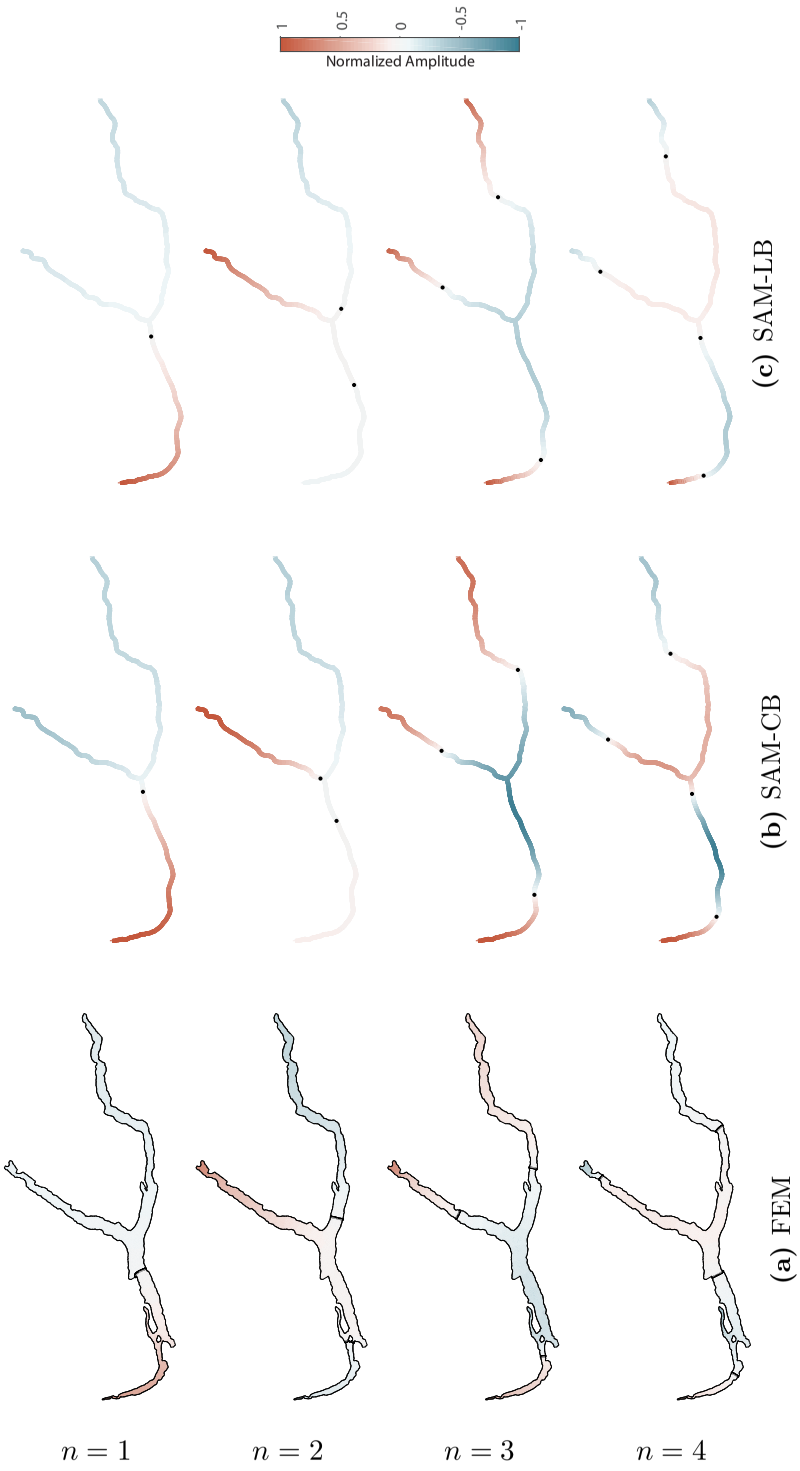

Figure 3.4: Mode-shapes in Quesnel Lake predicted by (a) The FEM model, (b) SAM-CB, and (c) SAM-LB corresponding to the labelled mode numbers, n. Deflections are normalized between -1 (blue) and 1 (red), and nodes are indicated by black contours or dots.

Arm.

As with Lake Como, SAM does produce qualitatively accurate mode-shapes with both SAM-CB and SAM-LB depth variations in Quesnel Lake (Figure 3.4), though these are less accurate within Quesnel Lake than they were in Lake Como. Whereas in Lake Como, there was very little difference between the positions of the nodes between the FEM, SAM-CB, and SAM-LB models, in Quesnel Lake the node locations do experience some travel between models, particularly in the second mode. The FEM model predicts that the second mode has one node that is located on the sill near Cariboo Island, and a second node near the entrance of the East Arm. In both SAM-CB and SAM-LB, the Cariboo Island node has moved eastward and is located midway along the West Arm; in SAM-CB the movement of the node near the entrance to the East Arm has caused it to shift around the corner into the entrance of the North Arm, thus incorrectly predicting the phase relationship between the terminus of the North and West Arms.

The differences between observed and predicted modal periods and mode shapes suggest that the modelled response of Quesnel Lake is more sensitive to depth variation than Lake Como. One possible explanation for this increased sensitivity is the influence of the sill and constriction at Cariboo Island. Partial wave reflections at this location may act to modify the standing wave modes of the lake. The present study does not have a mechanism to directly investigate the impact of a sill on the barotropic response, but it is noted that neither of the instances of SAM (-CB or -LB) include the influence of the sill, whereas the FEM does. Additionally, the second mode, where SAM and FEM mode-shape results have the greatest difference, the nodal line predicted by the FEM is directly over the sill; it is unclear if this is a coincidence or not.

3.3.3 Accuracy of the simplified analytical model

Despite the fact that predictions are less accurate in Quesnel Lake than they are in Lake Como, overall the mode-shapes predicted by SAM showed good agreement with the FEM model in both lakes. In most cases, SAM accurately predicted the phase relation between arms, and the number and approximate location of all nodal lines. The primary difference between mode-shapes predicted by SAM-CB versus SAM-LB is the amplitude of the deflections away from the terminus of the arms. In both lakes, SAM-LB predicted lower deflections away from the ends of the arms which more accurately captured the variation in deflection amplitude exhibited by the FEM predicted mode-shapes when compared to SAM-CB model. This behaviour can be

attributed to the spatially decreasing amplitude of oscillations in the functions η when the lake depth $H(x)$ is increasing away from the ends of the arms (see Section 2.3.2 in Chapter 2 for more details). Note in particular the differences between the results of SAM-CB and SAM-LB in the deflection at the anti-nodes in the third and fourth modes in both lakes. The fact that SAM reproduces this mode localization is taken as another indicator of its success.

As expected, SAM was also able to predict the periods of the lowest modes, which are relatively insensitive to depth. The inability of SAM-CB to predict the periods of higher modes is a reflection of the simplifications made to account for depth variation. It is expected that a model that is able to include depth variation would more accurately predict mode-shapes and periods of higher modes; however, energy is typically contained in the lowest modes and so accurate representation of higher modes may not be a major concern in most lakes.

3.4 Discussion

3.4.1 General behaviours of multi-armed lakes

There are a number of strong similarities between the barotropic mode-shapes predicted for both Lake Como and Quesnel Lake. From theses similarities, some general statements are made about the response of fjord-type multi-armed lakes.

In both lakes, the first mode is governed by high deflection and a single node in the arm with the largest value of τ_i (the $i = 1$ arm; coincidentally, the western arm of each lake). Out-of-phase deflections are distributed between the remaining two arms of the lake. In Quesnel Lake, the value of τ_1 in the West Arm is greatest because that arm is relatively shallow compared to the other two; the much longer extents of the East and North Arms ($i = 2, 3$) results in low deflections in those arms in order to conserve mass. In Lake Como, where all of the arms have similar lengths, the negative deflection in each of the North and East Arms ($i = 2, 3$) accounts for roughly half of the positive deflection in the Como Branch ($i = 1$). The horizontal angles formed by the arms as they extend from central junction slightly obfuscates the fact that in both of these lakes the fundamental behaviour is roughly an east-west rocking of the surface.

Section 2.3.1 suggests that the period of the fundamental mode can be estimated with Merian's formula applied along the longest extent of the lake. This implies that the fundamental mode should be largely described as a

simple oscillation of the two arms that form that extent, though other arms will still be included in the response. The nodal line for the first mode is expected to occur in the arms with the highest value of τ_i which is consistent with the results in both Lake Como and Quesnel Lake. This mode is can be thought of as a linear co-oscillation of that arm out-of-phase with the rest of the lake.

A similar response is seen in the first horizontal mode for other multi-armed and complex lakes. In a three-layer model, both the V1H1 and V2H1 baroclinic responses of Nechako Reservoir are characterized by linear oscillations in which Natalkuz Lake is out-of-phase from Knewstubb Lake (an overall east-west oscillation). In Lake Onega the first mode is marked by a high deflection in Povenetskiy Bay with a nodal line in that arm. All other arms and bays of the lake oscillate together with the main body of the lake (Rudnev et al., 1995). The oscillation appears to be a simple north-south rocking of the entire lake. Lake Te Anau (Carter and Lane, 1996) and Clear Lake (Rueda and Schladow, 2002) have first modes that are also described as simple linear oscillations despite the complex shape of those lakes.

In Lake Como, the second mode corresponds to the mixed TM type response predicted by SAM, in which only the North Arm and the Lecco Branch are active. Because Quesnel Lake is not expected to have a decoupled response, we don't necessarily expect strong agreement between the two lakes for this mode. Indeed, in Quesnel Lake the second mode has non-zero deflections across all arms of the lake; however, the overall response is still largely characterized as an oscillation of only two arms. For both Lake Como and Quesnel Lake, the two arms that characterize the second mode are $i = 2, 3$; that is, the two arms most active in the mode-2 response are the ones that were not dominant in the mode-1 response. It is further noted that in both lakes, the two nodal lines appearing in the second mode do not occur within the same arm.

The third mode in both lakes is a radial mode with an anti-node near the geometric centre of the lake. For a lake with a geometry that conforms to the TE case, SAM predicts that the first whole-lake mode will have an anti-node at the confluence point. Neither of these lakes is described by the TE case, and the anti-node is not directly at the confluence point. Given that within each of the two lakes, all of the arm lengths are of the same order of magnitude, it is unsurprising that a response with a central anti-node may appear as the third mode. Nechako Reservoir, on the other hand, does not seem to have any radial mode of the same structure (Imam, 2012; Imam et al., 2017). In Nechako Reservoir, sidearms are relatively short compared to the total east-west extent of the lake so the mode-2 radial-like response is

simply analogous to the mode-2 response in simple elongated lakes.

In the fourth mode (and higher modes not shown), deflections become more complex and harder to describe. In both Lake Como and Quesnel Lake, the fourth mode has four nodal lines, and in both cases the distribution of these nodes is consistent: two nodes exist in the $i = 1$ arm (with the highest value of τ_i), and one node exists in each of the other two arms. An additional feature of these higher modes is that deflections are increasingly localized to the tips of the arms. This localization is actually expected, and can be explained in terms of the analytical model (see Section 2.3.2 in Chapter 2).

In simple elongated lakes, there is an expected one-to-one correspondence between mode number and the number of nodal lines. For the lakes described above, this is true for the first mode which contains a single nodal line in each case. For some complex geometries, this one-to-one correspondence is not true for higher modes. For example, Rudnev et al. (1995) labels two nodal lines in both the second and third modes of Lake Onega, and only three nodal lines exist in the fourth mode. However, the geometry of Lake Onega should not be classified strictly as a multi-armed lake due the the ambiguity between "arms" versus "bays", so the modes predicted may represent the influence other geometric features. In Nechako Reservoir, which conforms to the classification of fjord-type multi-armed geometry, the number of nodal lines observed in each baroclinic mode matches the horizontal mode number for the majority of modes shown (the only exception being the upper interface in the V1H5 response) (Imam, 2012; Imam et al., 2017) . In the present study, the one-to-one correspondence also holds.

The results suggest predictability of the locations of these nodes in lakes of this geometric class. As described, we observe that the first mode is a general Merian-type oscillation with a single node located in the the arm with the highest value of τ_i. The N^{th}-mode response of an N-armed lake will be a radial mode with a single modal line in every arm. The results here further suggest that the modes numbered $1 \leq n \leq N$ seem to have $0 - 1$ nodes per arm, and modes numbered $N \leq n \leq 2N$ will have $1 - 2$ nodes per arm, etc. These patterns likely arise because the values of τ_i are unequal but of the same order of magnitude for all arms. It is likely that in a case where one arm is disproportionately long or small, these descriptions would not be valid; in those cases, the longest extent of the lake may behave similarly to a simple elongated lake with limited modification by the smaller arm(s). Furthermore, in a fully decoupled case (the TE case), the placement and number of nodes will not follow this pattern; however, in that case it will be reasonably easy to predict where these nodes will occur. For high enough mode numbers it is expected that transverse modes and harbour-constrained

modes may erode these patterns just as they would in simple geometries.

3.4.2 The activation of higher modes

In both the FEM and SAM results, the distribution of barotropic seiche amplitude within the lake has considerable spatial variation. While the highest deflections are always present at one extremity of the lake for each of the modes, the distribution of out-of-phase deflections between arms of a lake may result in relatively low deflections in certain arms, even if a decoupled response is not present. For example, in the first mode of Lake Como the FEM predicts a maximal normalized deflection of +1 at the tip of the Como Branch, but the deflections at the tips of the Lecco Branch and the North Arm are only -0.39 and -0.52, respectively. Similar results are shown in Quesnel Lake. This energy distribution creates interesting questions in terms of which of the modes will be active in the lake response. In simple lakes, the dominant response is typically consistent with the fundamental mode for both barotropic and baroclinic modes (Mortimer, 1952). While this result has been attributed to resonance between temporal fluctuations of the wind forcing and the V1H1 period (e.g. Hutter et al., 1983) or the minimal damping of the V1H1 mode (e.g. Mortimer, 1952), Imam et al. (2017) suggests that instead, it is the spatial uniformity of the wind field that results in that mode being activate. In general, it is expected that the energy imparted to a given mode is related to the similarity of that mode to the spatial structure of the forcing mechanism (Guyennon et al., 2014; Shimizu et al., 2007). As a result, for multi-armed lakes in which the local topography may result in non-uniform wind fields, higher modes may become the dominant response.

An extension of this result is that wind storms localized to a single arm of a multi-arm lake have the potential to generate currents and displacements in other arms. The linearized problem is an initial-condition eigenvalue problem, so any initial wind set-up, $F_0(x, y)$, will be constructed by a linear combination of eigenmodes:

$$F_0(x, y) = \sum_{n=1}^{\infty} A_n \eta_n(x, y).$$

When forcing subsides and the surface is allowed to relax, these modes will oscillate with their distinct frequencies ω_n. In the TNE case, all modes $\eta_n(x, y)$ have deflections across the entire domain; at $t = 0$ these deflections may add to zero in some sub-domain, but because the modes all oscillate

with different frequencies, at some time $t > 0$ the modes will separate and so $h(x, y, t) \neq 0$ everywhere.

While not a general feature of multi-armed lakes, we speculate that the constriction near Cariboo Island may also contribute to the activation of higher modes in Quesnel Lake. In a study of Lake Winnipeg, Einarsson and Lowe (1968) discuss the impact of constrictions in that lake on barotropic set-up. Those authors suggest that constrictions in Lake Winnipeg induce a time-lag on the steady-state set up of the lake. The transient set-up would include a state in which each individual basin of the lake undergoes its own set up (see Figure 3.5). Imam et al. (2017) notes similar local tilts of the metalimnion of separated basins in Nechako Reservoir. The processes described by both Einarsson and Lowe (1968) and Imam et al. (2017) have the potential to lead to an initial set-up condition in Quesnel Lake that matches Figure 3.5. Relaxation of a set-up that consists of basin-specific tilts of the water surface is likely to impart energy to higher modes in the same manner that those modes are activated when their mode-shapes reflect the spatial variation of forcing. This may account for the high energy is modes with periods ≤ 30 minutes observed in Figure 3.3.

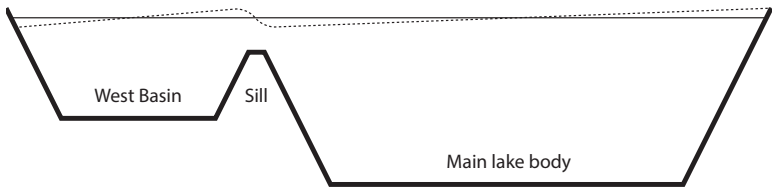

Figure 3.5: Schematic representation of a possible transient set-up of Quesnel Lake. The solid black line represents the undisturbed water surface, while the dashed line shows the initial stage of set-up.

3.5 Conclusions

By comparing the spatial structure of the mode-shapes of both Quesnel Lake and Lake Como, we've been able to infer some general patterns in the structure of the modes in Y-shaped lakes, or multi-armed lakes with any number of arms. The results justify the use of a simplified analytical model (SAM). As seen here, the first fundamental mode in these lakes does not differ substantially from simple elongated lakes and acts as a simple linear oscillation between the arm with the highest value of τ_i and the remainder of the lake. However, due to the varied directions at which arms radiate

from the confluence point, it may be difficult to recognize this mode as a simple co-oscillation without considering the results of SAM. The locations of nodes and corresponding spatial distribution in surface deflection in higher modes may not be easy to intuit, but the SAM provides a relatively easy method by which to predict these mode-shapes. The results show that the one-to-one correspondence between mode number and the number of nodal lines observed in elongated lakes appears to also be a feature of multi-armed lakes of the TNE and TM classes, though the inclusion of harbour-type modes and transverse modes will degrade that pattern at high enough mode numbers. Numerical modelling shows the localization of deflections to the terminus of arms at higher mode numbers for both lakes. This behaviour is explained analytically by SAM, and is expected to be a general feature of both simple and multi-armed lakes.

One important result of SAM is the possibility of a decoupled response in one or more arms of the lake. Specifically, the relative values of a parameter $\tau_i = L_i(gH_{0,i})^{-1/2}$, which is the travel time of a shallow water wave in the i^{th} arm, determines if such a behaviour will occur. If $\tau_1 \neq \tau_2 \neq \tau_3$ (called the TNE case), then no decoupling will occur, and all modes will act as whole-lake modes. Alternatively, if $\tau_i = \tau_j$ for a given subset of arms of the lake (called the TM case) then there will be some modes that act only across the arms i and j with a node at the confluence point, and all other arms will be decoupled from the response. When all arms have equal values of τ_i ($\tau_1 = \tau_2 = \tau_3$, called the TE case), multiple sets of decoupled modes will occur. In Lake Como, the wave-travel-times in the North Arm and Lecco Branch are equal, and the mode-2 response is an oscillation of only these two arms with the Como Branch absent from the response. No decoupling is observed in Quesnel Lake which corresponds to a TNE case. Because SAM provides a geometric criterion to predict the possibility of decoupled arms, such predictions are possible for a given lake before a more detailed numerical analysis is completed.

Even in lakes where decoupling or arms is not expected to occur, this study shows that seiche modes in multi-armed lakes do exhibit considerable spatial variation in modal amplitudes (and corresponding velocities). This spatial heterogeneity of mode-shapes of both barotropic and baroclinic modes has implications for water quality within multi-armed lakes due to the role of horizontal velocity in both resuspension and transport. Due to their short periods, horizontal velocities generated by the barotropic response can be comparable in magnitude to those caused by baroclinic seiches (Lemmin and Mortimer, 1986), and both have the capacity to resuspend bottom sediments in lakes (Bloesch, 1995; Chung et al., 2009; Gloor et al., 1994). These bottom

sediments are able to act as stores of nutrients or of harmful toxins (Chung et al., 2009), so resuspension is an important for both water quality and ecology. The spatial variation of seiche-induced horizontal velocities in multi-armed lakes (with decoupling of arms being an extreme example of spatial variation) can then lead to localized areas of resuspension. Baroclinic seiching is responsible for the transport of material through a lake (Hodges et al., 2000; Mortimer, 1952), so if there is a localized nutrient or pollution loading into a lake (i.e. from a river inflow or due to localized areas of resuspension), the spatial variation in internal currents and the decoupling of arms will determine whether that loading has the ability to impact the entire lake or only some subsection. In an extreme case, high loadings into an arm that is decoupled from the rest of the lake in the seiche response can limit mixing or flushing in that arm, and create localized pollution or eutrophication concerns.

Chapter 4

Conclusions

4.1 Summary and contributions

This study examined the free oscillatory response of lakes with multiple narrow, elongated arms. This was achieved through the use of an analytical description in an idealized case (Chapter 2), and a comparison of case studies conducted to two Y-shaped lakes (Chapter 3). The results of the study allow for some general statements to be made about this response.

Chapter 2 presents the development a simplified analytical model (SAM) for idealized, multi-armed lakes. This model considered bathymetric variation by describing the results in the cases of a constant bottom and a linearly varying bottom, and presenting the results of an asymptotic approximation for an arbitrary bottom. It was found that regardless of the specific form of depth variation being considered, the relative values of a single parameter τ_i, which represents the travel time of a progressive shallow-water wave along the i^{th} arm of the lake, can be used to classify the lake into two behavioural regimes: lakes with decoupled modes, and lakes with only whole-lake modes.

While these idealized results were valuable, it was also necessary to examine realistic bathymetries. Chapter 3 compared both field results, numerically modelled results, and SAM results of two Y-shaped lakes: Quesnel Lake and Lake Como. The results provide justification of the ability of the SAM to both predict and explain the seiche modes of these lakes.

Of particular interest in this study is the explanation in Chapter 2 of the potential decoupled response in multi-armed lakes. While this behaviour was previously observed in Lake Como (Buzzi et al., 1997; Guyennon et al., 2014), it was absent from Knewstubb and Natalkuz Lakes (Imam, 2012), leading to questions about when such a behaviour might be expected to occur in general, or whether Lake Como presented an a-typical case. Not only does the SAM provide an explanation for why this decoupling happens, but also gives a criteria for predicting whether it will occur in a given lake. If the wave travel time, τ_i, is equal in two arms of a multi-armed lake, the resulting standing wave mode produced by those two arms will have a node at the confluence point of all of the arms. With zero-deflection at the junction,

all other arms will be absent (decoupled) in the response for that mode. When applied to Lake Como in Chapter 3, this prediction is consistent with observed behaviour; conversely, consistent with the SAM predictions, Quesnel Lake is not expected to exhbit any decoupled behaviour.

The results of this study also provide some basis for predicting the mode-shape of the fundamental mode. As demonstrated by Malinina and Solntseva (1972), Laval et al. (2008) and Imam et al. (2013b), the intuition of some researchers in trying to predict the fundamental period of a multi-armed lake is to apply Merian's formula along the longest continuous extent of the lake. The results of the SAM suggest that even for lakes in which none of the arms are decoupled, applying Merian's formula as suggested may provide a reasonable "first guess" of the fundamental seiche period. This first mode will then conform to a general "linear" oscillation in which the arm with the highest value of τ_i exhibits motion out-of-phase from the remaining arms of the lake in a back-and-forth rocking analogous to simple elongated lakes. The studies of Lakes Como and Quesnel in Chapter 3 confirm that the first mode is well described by this general linear oscillation, with a single nodal line in the arm that has the highest value of τ_i.

An additional interesting result of this study is the observations in Chapter 3 of the localization of deflections for higher modes. In this geometry where motions are primarily longitudinal, this localization resulted in high deflections near the terminus of different arms, with a relatively inert lake body. The SAM provides an analytical explanation for this in terms of the structure of mode-shapes attributed to shoalling bathymetries versus flat-bottomed. An extension of the SAM to include width variation (see Section 2.3.2) would cause an exaggeration of these results. In more complex two-dimensional domains, this mode localization may be related to the bay and harbour modes observed in locations such as Lake Onega (Rudnev et al., 1995), or Flathead Lake (Kirillin et al., 2014).

4.2 Future work

4.2.1 Additional study of Quesnel Lake and Lake Como

Barotropic modes

Buzzi et al. (1997) provides a detailed study of barotropic modes within Lake Como. The modelling work performed by those authors is repeated in Chapter 3 with a higher mesh density, and more context is provided to explain the structure of the predicted modes. While this study appears

consistent with the modes observed by Buzzi et al. (1997) during a field study, the width of the spectral band centred near 35-minutes in the observed data obstructs the ability to differentiate between the first and second modes. Furthermore, because of the the lack of spatial coverage of field data, it is not possible to verify the predicted mode-shapes. In order to fully validate the model output, it would be valuable to perform an additional field study of Lake Como. Such a study would entail a spatial array of water level sensors (at minimum, one at the terminus of each arm); these sensors would need to record at a high enough frequency and for a long enough interval to allow for the separation of these modes in the spectral response.

The present work provides a characterization of the barotropic modes in Quesnel Lake that is consistent with both the observed oscillatory periods and the spatial distribution of spectral energy signals. Nonetheless, there are still unanswered questions regarding the barotropic response of the lake. In particular, it would be interesting to better understand the role of the constriction at Cariboo Island on seiche modes. Chapter 3 provides some circumstantial evidence that the form of the free modes is modified by the inclusion of the constriction, possibly due to partial reflections. A more robust analysis of this effect can be undertaken using the finite element method (FEM) numerical model used in Chapter 3. An artificial lake bathymetry can be constructed in which Cariboo Island is removed and the sill is smoothed out, effectively removing the constriction; a comparison of the appliction of the FEM model to this constructed bathymetry with the results presented in Chapter 3 would help explain the impact of the sill on the mode-shapes and periods of the free modes.

As described in Chapter 3, the sill may also have an impact on the activation of higher barotropic modes. Given that the observed spectral response of Quesnel Lake agrees with the periods predicted by the FEM model, this time lag may be negligible compared to the period of the barotropic modes. Even if the time lag does not impact the periods of the barotropic modes, the transient form of the set-up depicted in Figure 3.5 may occur in reaction to short-duration wind gusts. Some of the energetic peaks at higher frequencies in the spectral response of Quesnel Lake (Figure 3.3) may be attributed to a reaction to such a partially set-up surface.

Baroclinic modes in Quesnel Lake

Chapter 3 provides a characterization of barotropic modes in Quesnel Lake. While these are interesting in explaining the behaviour of multi-armed lakes, barotropic motions may not contribute to mass transport to the same degree

as baroclinic motions. Laval et al. (2008) found that baroclinic motions can have a profound impact on the exchange of deep water between basins of the lake, but as of yet no characterization has been made of these internal modes. While it would be of interest to apply the FEM and SAM models discussed in the present study to the baroclinic response of Quesnel Lake directly, it may first be necessary to further understand the role of the sill at Cariboo Island in modifying baroclinic modes.

The transient surface set-up in lakes that contain constrictions described by Einarsson and Lowe (1968), and depicted schematically in Figure 3.5 may similarly apply to the baroclinic set-up. The so-called "split layer" observed in Lake Constance by Appt et al. (2004) is likely an extreme example of such a set-up, in which non-linear effects cause the interface to surface in the vicinity of a sill. Imam (2012, Chapter 6) further discussed the possibility of a split layer in Knewstubb and Natalkuz lakes, and argues that the condition to describe it's occurrence should be $W_d < 1 < W_u$, where $W_{u,d}$ are the Wedderburn numbers in the upwind (u) and downwind basins (d). In Lake Constance, the subsistence of the wind forcing during the split layer event was associated with the generation of an internal surge. It would be instructive to consider that result in the context of the degeneration regimes described by Horn et al. (2001); it is possible that if the upwelling was less drastic, the set-up would have relaxed instead into a decoupled set of standing waves constrained to each of the two basins of the lake. If the existence of a constriction can lead to the decoupling of baroclinic seiche modes between basins, it would have a strong impact on the choices of geometry used in predicting the free response modes.

4.2.2 Forced response of multi-armed lakes

In basins of simple geometry, energy is primarily contained in the fundamental horizontal mode for both barotropic and baroclinic seiching (Mortimer, 1952). In more complex lakes, this may not be the case. It is believed that for lakes of complex geometry, the energy imparted to a particular barotropic mode will be based on the similarity of the corresponding mode-shape to the spatial distribution of the forcing pattern (Guyennon et al., 2014). Imam (2012) suggests that the activation of baroclinic modes will be related to resonance conditions between the wind timeseries and the free modes of the lake. His study, however, did not account for the full spatial variation of the wind field.

Whether through a hydrodynamic model such as ELCOM (Hodges et al., 2000) for FVCOM (Chen et al., 2003) or a semi-numeric model such as the

impulsively forced TVC developed by Imam (2012); Imam et al. (2013b), it would be interesting to evaluate the the forced response of a multi-armed lake with the specific goal of understanding the role of the different arms on the response and activation of different modes. Such a study would likely rely on a more complete picture of the spatial variability of the wind forcing. Laval et al. (2008) suggests that the mountainous terrain surrounding Quesnel Lake acts to channel the wind along the local thalweg of each arm. As part of the present study, this author did attempt to analyse data collected at lakeshore meteorological stations at Quesnel Lake in an effort to better describe the spatial and temporal variation of the wind forcing, and link those results to observed temporal variation in the spectral energy of different barotropic modes within the lake. While those results provided evidence that agreed with the assertions of Laval et al. (2008), the lack of wind data that was coincident with recordings of water level in the lake prevented a robust analysis. No definitive conclusions were made.

Given that fjord-type lakes typically sit in deep valleys carved by the same glaciers that formed the lakes themselves, the impact of topography on local wind patterns is likely to be an underlying question in all force-response models of these lakes. Using an array of meteorological stations, Ludwig et al. (2004) provides one framework for evaluating these data using Empirical Orthogonal Functions (EOFs), which may be of value in describing topographic channelling. A more complete study of topographic wind channelling over a lake and the resulting effects on baroclinic circulation has recently been completed on Lake Iseo (Valerio et al., 2017). Those authors simulated the wind field using the Weather Research and Forecasting (WRF) atmospheric model, and their results indicate spatial variation of the wind field had an impact on the energy imparted to baroclinic modes.

In multi-armed lakes, a more complete understanding of the spatial variation of the wind (through modelling or field study) may reveal wind forcing that is locally constrained or may be channelled in different directions along different arms of the lake. Such patterns could result in some mode other than the fundamental mode being the primary energetic mode of the lake.

4.2.3 The use of simplified analytical models in predicting seiche response

Appliction of the SAM to other lakes

It would be very interesting to apply the SAM to other multi-armed lakes. Two potential contenders for which the SAM may provide valuable insight are Shuswap Lake in British Columbia, and Keuaka Lake in New York.

Shuswap Lake has four arms extending from a central junction. A constriction at the junction separates the lake into two connected longitudinal extents. Assuming that depth doesn't vary drastically through the lake, the lengths of the arms can be used to infer whether τ_i would be expected to be equal (the TE case) or unequal (the TNE case), or a mixture of the two (the TM case). In fact, a cursory investigation suggests a TM case may occur. Given the constriction, and the potential for some arms decoupled from the response, it would be interesting to see if all of the possible free modes are realized in the lake.

Like Lake Como and Quesnel Lake, Keuka Lake is Y-shaped. The lake has two shorter arms that extend continuously in a roughly north-south direction, and a longer arm that branches out almost perpendicular to the other two before turning in a north-east direction. While the SAM does not consider the relative angles of the arms as they extend from the junction, it is reasonable to expect that response of the lake may favour the activation of a mode along a continuous extent, compared to one that needs to turn a corner. Based on the results presented in Chapter 3, one might expect that the fundamental mode in Kueka Lake would be a co-oscillation of the north-east arm with the main body of the lake in an overall east-west rocking motion. However, a field study may find that the second mode, which is likely a north-south oscillation of the two shorter arms with relatively low deflection in the north-east arm (possibly even a a fully decoupled north-east arm), may be the dominant mode within the lake.

Development of models for other geometric features

The present SAM considers the effects of multiple arms on the seiche response of a lake. While this is of interest, there are other geometric features that may be of similar interest to other researchers. By considering the process used to develop the model described in Chapter 2, it may be possible to construct SAM's for other geometries as well.

Ultimately, the development of the SAM for multi-armed lakes is limited in its application by the number of multi-armed lakes of interest or importance.

Nonetheless, the success of this model in providing context and understanding for the barotropic modes observed in Lake Como and Quesnel Lake, and the framework it provides for understanding those modes in other multi-armed lakes shows the value in using simple models to describe the important geometric features in isolation.

Bibliography

K. Aichi. On the internal seiches. *Tokyo Sugaku-Buturigakkwai Kizi Dai 2 Ki*, 9(20):464–478, 1918a. doi: 10.11429/ptmps1907.9.20_464.

K. Aichi. Calculation of the period of the internal seiches for various lakes, and sea. *Tokyo Sugaku-Buturigakkwai Kizi Dai 2 Ki*, 9(20):478–485, 1918b. doi: 10.11429/ptmps1907.9.20_478.

J. Alberty, C. Carstensen, and S. A. Funken. Remarks around 50 lines of matlab: short finite element implementation. *Numerical Algorithms*, 20 (2-3):117–137, 1999. doi: 10.1023/A:1019155918070.

J. Appt, J. Imberger, and H. Kobus. Basin-scale motion in stratified Upper Lake Constance. *Limnology and Oceanography*, 49(4):919–933, jul 2004. doi: 10.4319/lo.2004.49.4.0919.

N. Balmforth, J. Von Hardenberg, and R. Zammett. Dam-breaking seiches. *Journal of Fluid Mechanics*, 628:1–21, 2009. doi: 10.1017/S0022112009005825.

A. Barberopoulou. A seiche hazard study for Lake Union, Seattle, Washington. *Bulletin of the Seismological Society of America*, 98(4):1837–1848, 2008. doi: 10.1785/0120070153.

C. Bender and S. Orszag. *Advanced Mathematical Methods for Scientists and Engineers I: Asymptotic Methods and Perturbation Theory.* Springer, 1999. ISBN 978-1-4419-3187-0. doi: 10.1007/978-1-4757-3069-2_5.

J. Bloesch. Mechanisms, measurement and importance of sediment resuspension in lakes. *Marine and Freshwater Research*, 46(1):295–304, 1995. doi: 10.1071/MF9950295.

W. E. Boyce and R. C. DiPrima. *Elementary Differential Equations and Boundary Value Problems.* John Wiley & Sons Inc, 1986. ISBN 0-471-07895-6. doi: 10.2307/2314317.

F. Buzzi, G. Gerosa, and G. Saldavè. Descrizione e analisi di alcuni aspetti limnologici e idrodinamici del Lago di Como. *Documenta Ist. Ital. Idrobiol*, 61:93–115, 1997.

P. Caloi and M. Spadea. Le sesse del lago di Como — Parte I. *Annals of Geophysics*, 11(3-4):191–198, 1958. doi: 10.4401/ag-5821.

G. Carter and M. Lane. Modelling surface oscillations in New Zealand lakes. *New Zealand Journal of Marine and Freshwater Research*, 30(3):341–353, 1996. doi: 10.1080/00288330.1996.9516721.

C. Chen, H. Liu, and R. C. Beardsley. An unstructured grid, finite-volume, three-dimensional, primitive equations ocean model: application to coastal ocean and estuaries. *Journal of atmospheric and oceanic technology*, 20(1): 159–186, 2003. doi: 10.1175/1520-0426(2003)020⟨0159:AUGFVT⟩2.0.CO; 2.

G. Chrystal. XXV.—On the hydrodynamical theory of seiches. *Transactions of the Royal Society of Edinburgh*, 41(3):599–649, 1905. doi: 10.1017/S0080456800035523.

G. Chrystal. XX.—an investigation of the seiches of Loch Earn by the Scottish Lake Survey. Part III.: Observations to determine the periods and nodes.—Part IV.: Effect of meteorological conditions upon the denivellation of lakes.—Part V.: Mathematical appendix on the effect of pressure disturbances upon the seiches in a symmetric parabolic lake. *Transactions of the Royal Society of Edinburgh*, 46(03):455–517, 1908. doi: 10.1017/S0080456800003781.

G. Chrystal and J. Murray. XIV.—an investigation of the seiches of Loch Earn by the Scottish Lake Survey Part I.: Limnographic instruments and methods of observation. Part II.: Preliminary limnographic observations on Loch Earn. *Transactions of the Royal Society of Edinburgh*, 45(02): 361–396, 1907. doi: 10.1017/s0080456800022778.

G. Chrystal and E. M. Wedderburn. XXXII.—calculation of the periods and nodes of Lochs Earn and Treig, from the bathymetric data of the Scottish Lake Survey. *Transactions of the Royal Society of Edinburgh*, 41 (03):823–850, 1905. doi: 10.1017/s0080456800035596.

E. G. Chung, F. A. Bombardelli, and S. G. Schladow. Sediment resuspension in a shallow lake. *Water Resources Research*, 45(5), 2009. doi: 10.1029/2007WR006585.

G. Csanady. Hydrodynamics of large lakes. *Annual Review of Fluid Mechanics*, 7(1):357–386, 1975. doi: 10.1146/annurev.fl.07.010175.002041.

A. Defant. Neue methode zur ermittlung der eigenschwingungen (seiches) von abgeschlossenen wassermassen (seen, buchten, usw.). *Ann. Hydrogr*, 46:78–85, 1918.

A. Defant. *Physical Oceanography*, chapter Long Waves in Canals and Standing Waves in Entirely or Partly Closed Basins, pages 142–244. Pergamon Press, 1960.

A. Dorostkar and L. Boegman. Internal hydraulic jumps in a long narrow lake. *Limnology and Oceanography*, 58(1):153–172, 2013. doi: 10.4319/lo.2013.58.1.0153.

E. Einarsson and A. Lowe. Seiches and set-up on Lake Winnipeg. *Limnology and Oceanography*, 13(2):257–271, 1968. doi: 10.4319/lo.1968.13.2.0257.

W. N. Everitt. Charles Sturm and the development of Sturm-Liouville theory in the years 1900 to 1950. In *Sturm-Liouville Theory*, pages 45–74. Springer, 2005. doi: 10.1007/3-7643-7359-8_3.

D. M. Farmer. Observations of long nonlinear internal waves in a lake. *Journal of Physical Oceanography*, 8(1):63–73, 1978. doi: 10.1175/1520-0485(1978)008⟨0063:OOLNIW⟩2.0.CO;2.

F.-A. Forel. La formule des seiches. *Archives des sciences physiques et naturelles*, 1876.

M. Gloor, A. Wüest, and M. Münnich. Benthic boundary mixing and resuspension induced by internal seiches. *Hydrobiologia*, 284(1):59–68, 1994. doi: 10.1007/BF00005731.

G. Green. On the motion of waves in a variable canal of small depth and width. *Transactions of the Cambridge Philosophical Society*, 6:457, 1837.

N. Guyennon, G. Valerio, F. Salerno, M. Pilotti, G. Tartari, and D. Copetti. Internal wave weather heterogeneity in a deep multi-basin subalpine lake resulting from wavelet transform and numerical analysis. *Advances in Water Resources*, 71:149–161, 2014. doi: 10.1016/j.advwatres.2014.06.013.

J. Halm. XXVI.—on a group of linear differential equations of the 2nd order, including Professor Chrystal's seiche-equations. *Earth and Environmental Science Transactions of The Royal Society of Edinburgh*, 41(3):651–676, 1905. doi: 10.1017/S0080456800035535.

P. F. Hamblin. Short period tides in lake ontario. In *IN: PROCEEDINGS, SEVENTEENTH CONFERENCE ON GREAT LAKES RESEARCH, PART 2*, 1974.

N. S. Heaps and A. Ramsbottom. Wind effects on the water in a narrow two-layered lake. *Philosophical Transactions of the Royal Society of London A: Mathematical, Physical and Engineering Sciences*, 259(1102):391–430, 1966. doi: 10.1098/rsta.1966.0021.

E. J. Hinch. *Perturbation Methods*. Cambridge University Press, 1991. ISBN 0-521-37310-7. doi: https://doi.org/10.1017/CBO9781139172189.

D. Hinton. Sturms 1836 oscillation results evolution of the theory. In *Sturm-Liouville theory*, pages 1–27. Springer, 2005. doi: 10.1007/3-7643-7359-8_1.

B. R. Hodges, J. Imberger, A. Saggio, and K. B. Winters. Modeling basin-scale internal waves in a stratified lake. *Limnology and oceanography*, 45 (7):1603–1620, 2000. doi: 10.4319/lo.2000.45.7.1603.

D. Horn, J. Imberger, and G. Ivey. The degeneration of large-scale interfacial gravity waves in lakes. *Journal of Fluid Mechanics*, 434:181–207, 2001. doi: 10.1017/S0022112001003536.

K. Hutter, G. Raggio, C. Bucher, and G. Salvadè. The surface seiches of Lake of Zürich. *Schweizerische Zeitschrift für Hydrologie*, 44(2):423–454, 1982. doi: 10.1007/BF02502301.

K. Hutter, G. Salvadè, and D. Schwab. On internal wave dynamics in the northern basin of the lake of lugano. *Geophysical & Astrophysical Fluid Dynamics*, 27(3-4):299–336, 1983. doi: 10.1080/03091928308210131.

K. Hutter, Y. Wang, and I. P. Chubarenko. *Physics of Lakes Vol. 1*. Springer-Verlag GmbH, 2010. ISBN 978-3-642-15177-4. doi: 10.1007/978-3-642-15178-1.

K. Hutter, Y. Wang, and I. P. Chubarenko. *Physics of lakes Vol. 2*. Advances in geophysical and environmental mechanics and mathematics. Springer, Heidelberg [u.a.], 2011. ISBN 9783642191114. doi: 10.1007/978-3-642-19112-1.

Y. E. Imam. *Modal decomposition of the baroclinic response to wind in elongated lakes*. PhD thesis, University of British Columbia, 2012.

Y. E. Imam, B. Laval, and G. Lawrence. The baroclinic response to wind in a small two-basin lake. *Aquatic sciences*, 75(2):213–233, 2013a. doi: 10.1007/s00027-012-0268-1.

Y. E. Imam, B. Laval, R. Pieters, and G. Lawrence. The strongly damped baroclinic response to wind in a multibasin reservoir. *Limnology and Oceanography*, 58(4):1243–1258, 2013b. doi: 10.4319/lo.2013.58.4.1243.

Y. E. Imam, B. Laval, R. Pieters, and G. Lawrence. The baroclinic response to wind in a multi-arm multi-basin reservoir. [In preparation for submission to The Journal of Limnology and Oceanography], 2017.

G. Kirillin, M. Lorang, T. Lippmann, C. Gotschalk, and S. Schimmelpfennig. Surface seiches in Flathead Lake. *Hydrology and Earth System Sciences Discussions*, 11(12):13541–13570, 2014. doi: 10.5194/hess-19-2605-2015.

E. A. Kulikov, A. B. Rabinovich, R. E. Thomson, and B. D. Bornhold. The landslide tsunami of November 3 1994 Skagway harbor Alaska. *Journal of Geophysical Research Oceans*, 101(C3):6609–6615, 1996. doi: 10.1029/95JC03562.

B. E. Laval, J. Morrison, D. J. Potts, E. C. Carmack, S. Vagle, C. James, F. A. McLaughlin, and M. Foreman. Wind-driven summertime upwelling in a fjord-type lake and its impact on downstream river conditions: Quesnel Lake and river, British Columbia, Canada. *Journal of Great Lakes Research*, 34(1):189–203, 2008. doi: 10.3394/0380-1330(2008)34[189:wsuiaf]2.0.co;2.

B. E. Laval, S. Vagle, D. Potts, J. Morrison, G. Sentlinger, C. James, F. McLaughlin, and E. C. Carmack. The joint effects of riverine, thermal, and wind forcing on a temperate fjord lake: Quesnel lake, canada. *Journal of Great Lakes Research*, 38(3):540–549, sep 2012. doi: 10.1016/j.jglr.2012.06.007.

P. LeBlond and L. Mysak. *Waves in the Ocean*. Elsevier, New York, 1978. doi: 10.1093/gji/57.3.748-a.

U. Lemmin and C. H. Mortimer. Tests of an extension to internal seiches of defant's procedure for determination of surface seiche characteristics in real lakes. *Limnology and oceanography*, 31(6):1207–1231, 1986. doi: 10.4319/lo.1986.31.6.1207.

M. S. Longuet-Higgins. Water movements in lakes during summer stratification; evidence from the distribution of temperature in Windermere:

Appendix: Oscillations in a three-layered stratified basin. *Philosophical Transactions of the Royal Society of London. Series B, Biological Sciences*, pages 399–404, 1952. doi: 10.1098/rstb.1952.0005.

F. L. Ludwig, J. Horel, and C. D. Whiteman. Using eof analysis to identify important surface wind patterns in mountain valleys. *Journal of Applied Meteorology*, 43(7):969–983, 2004. doi: 10.1175/1520-0450(2004)043⟨0969:ueatii⟩2.0.co;2.

T. Malinina and N. Solntseva. The seiches of Lake Onega. water mass dynamics of Lake Onega. *Nauka*, pages 40–74, 1972.

J. R. Merian. *Über die Bewegung Tropfbarer Flüssigkeiten in Gefäßen*. Schweighauser, Basel, 1828.

S. Morillo, J. Imberger, J. P. Antenucci, and D. Copetti. Using impellers to distribute local nutrient loadings in a stratified lake: Lake Como, Italy. *Journal of Hydraulic Engineering*, 135(7):564–574, 2009. doi: 10.1061/(asce)hy.1943-7900.0000048.

C. Mortimer. Strategies for coupling data collection and analysis with dynamic modelling of lake motions. *Developments in Water Science*, 11: 183–222, 1979. doi: 10.1016/S0167-5648(08)70395-2.

C. H. Mortimer. Water movements in lakes during summer stratification; evidence from the distribution of temperature in Windermere. *Philosophical Transactions of the Royal Society of London B: Biological Sciences*, 236 (635):355–398, 1952. doi: 10.1098/rstb.1952.0005.

J. Murray. On the effects of winds on the distribution of temperature in the sea-and fresh-water lochs of the west of Scotland. *The Scottish Geographical Magazine*, 4(7):345–347, 1888. doi: 10.1080/14702548808554534.

G. Neumann. Die impedanz mechanischer schwingungssysteme und ihre anwendung auf die theorie der seiches. *Ann. Hydrogr. u. marit. Meteorol*, 65, 1944.

R. Ortiz, A. Marin, and J. Rodriguez. Natural vibrations of the shallow water equation. *British Journal of Mathematics and Computer Science*, 3 (4):649–654, 2013. doi: 10.9734/BJMCS/2013/4465.

R. Pieters and G. A. Lawrence. Physical processes and meromixis in pit lakes subject to ice cover. *Canadian Journal of Civil Engineering*, 41(6): 569–578, 2014. doi: 10.1139/cjce-2012-0132.

H. J. Priestley. On the oscillations of superposed fluids. *Cambridge Philosophical Society. Proceedings*, 15:297–309, 1909.

J. Proudman. Free and forced longitudinal tidal motion in a lake. *Proceedings of the London Mathematical Society*, 2(1):240–250, 1915. doi: 10.1112/plms/s2_14.1.240.

J. Proudman. *Dynamical oceanography*. Methuen, 1953.

S. Rudnev, G. Salvadè, K. Hutter, and F. Zamboni. External gravity oscillations in Lake Onega. *Annales Geophysicae*, 13(8):893–906, 1995. doi: 10.1007/s00585-995-0893-2.

F. J. Rueda and S. G. Schladow. Surface seiches in lakes of complex geometry. *Limnology and oceanography*, 47(3):906–910, 2002. doi: 10.4319/lo.2002.47.3.0906.

F. J. Rueda and S. G. Schladow. Dynamics of large polymictic lake. II: Numerical simulations. *Journal of Hydraulic Engineering*, 129(2):92–101, 2003. doi: 10.1061/(ASCE)0733-9429(2003)129:2(92).

N. Salmaso and R. Mosello. Limnological research in the deep southern subalpine lakes: synthesis, directions and perspectives. *Advances in Oceanography and Limnology*, 1(1):29–66, 2010. doi: 10.1080/19475721003735773.

A. Schneider. A note on eigenvalue problems with eigenvalue parameter in the boundary conditions. *Mathematische Zeitschrift*, 136(2):163–167, 1974.

D. J. Schwab. The free oscillations of Lake St. Clair : an application of Lanczos' procedure. Technical Report ERL-GLERL-32, Great Lakes Environmental Research Laboratory, 1980. URL `http://purl.access.gpo.gov/GPO/LPS94331`.

D. J. Schwab and D. B. Rao. Gravitational oscillations of Lake Huron, Saginaw Bay, Georgian Bay, and the North Channel. *Journal of Geophysical Research*, 82(15):2105–2116, may 1977. doi: 10.1029/jc082i015p02105.

K. Shimizu, J. Imberger, and M. Kumagai. Horizontal structure and excitation of primary motions in a strongly stratified lake. *Limnology and oceanography*, 52(6):2641–2655, 2007. doi: 10.4319/lo.2007.52.6.2641.

C. Stevens and J. Imberger. The initial response of a stratified lake to a surface shear stress. *Journal of Fluid Mechanics*, 312:39–66, 1996. doi: 10.1017/S0022112096001917.

G. Valerio, A. Cantelli, P. Monti, and G. Leuzzi. A modeling approach to identify the effective forcing exerted by wind on a prealpine lake surrounded by a complex topography. *Water Resources Research*, 2017. doi: 10.1002/2016wr020335.

D. C. Van Senden and D. M. Imboden. Internal seiche pumping between sill-separated basins. *Geophysical & Astrophysical Fluid Dynamics*, 48 (1-3):135–150, 1989. doi: 10.1080/03091928908219530.

E. Watson. Movements of the waters of Loch Ness, as indicated by temperature observations. *The Geographical Journal*, 24(4):430–437, 1904. doi: 10.2307/1775951.

E. Wedderburn. XVI.—the temperature of the fresh-water lochs of Scotland, with special reference to loch ness. with appendix containing observations made in Loch Ness by members of the Scottish Lake Survey. *Transactions of the Royal Society of Edinburgh*, 45(02):407–489, 1907. doi: 10.1017/S0370164600017235.

E. Wedderburn. Seiches. *Quarterly Journal of the Royal Meteorological Society*, 48(203):211–223, 1922. doi: 10.1002/qj.49704820302.

E. M. Wedderburn and A. M. Williams. XXII.—the temperature seiche. Part I. Temperature observations in the madsee, pomerania. Part II. Hydrodynamical theory of temperature oscillations in lakes. Part III. Calculation of the period of the temperature seiche in the madsee. Part IV. Experimental verification of the hydrodynamical theory of temperature seiches. *Transactions of the Royal Society of Edinburgh*, 47(04):619–642, 1911. doi: 10.1017/s0080456800003860.

R. G. Wetzel. *Limnology*. Saunders College Publishing, second edition edition, 1983. ISBN 0-03-057913-9. doi: 10.1016/B978-0-08-057439-4.50017-4.

B. Wilson. Seiches. *Advances in hydroscience*, 8:1–94, 1972.